Univerzita Karlova v Praze
Matematicko-fyzikální fakulta

DIZERTAČNÍ PRÁCE

Seismické lokální účinky (analýza dat a modelování)

Dott. in Fisica Arrigo Caserta

Školitel: prof. RNDr. Jiří Zahradník, DrSc.

Katedra geofyziky
V Holešovičkách 2
180 00 Praha 8

Praha, 2011

Charles University in Prague
Faculty of Mathematics and Physics

DOCTORAL THESIS

Seismic Site Effects (Data Analysis and Modelling)

by

Dott. in Fisica Arrigo Caserta

Supervisor: prof. RNDr. Jiří Zahradník, DrSc.

Department of Geophysics
V Holešovičkách 2
180 00 Praha 8
Czech Republic

Prague 2011

Contents

Acknowledgments

The candidate wishes to thank first of all his family and in particular his wife, Serenella, for having supported and encouraged him. He gratefully acknowledges Antonio Rovelli and Antonio Piersanti, research leading and research manager, respectively, of Istituto Nazionale di Geofisica e Vulcanologia sede di Roma, for having allowed and supported the candidate in achieving this not easy task. The manuscript was significantly improved by valuable comments and helpful discussion with Ivo Opršal and František Gallovič. Appreciation is expressed for Aladino Govoni's relevant help in planning and realizing the roman seismic array. Particular thank to Prof. Giuseppe Della Monica and his RomaTRE University team for array maintenance. Vittorio Ruggiero and Piero Lanucara together with Ivo Opršal have given a fundamental contribution in numerically simulating the soil shaking features. In the end the candidate would like to express his gratitude to his supervisor Jiří Zahradník ever available and patient in sharing his vast knowledge; the result is a lesson that goes well beyond the present Thesis. In addition to internal research funds by INGV, the present Thesis benefited from a partial funding by the Italian Minister for Research (MIUR) under two grants: FIRB and COFIN. The Thesis benefited also from funds by the projects GACR 205/07/0502, GACR 210/11/0854 and MSM 0021620860 (Czech Republic).

Prohlašuji, že jsem tuto disertační práci vypracoval samostatně a výhradně s použitím citovaných pramenů, literatury a dalších odborných zdrojů.

Beru na vědomí, že se na moji práci vztahují práva a povinnosti vyplývající ze zákona č. 121/2000 Sb., autorského zákona v platném znění, zejména skutečnost, že Univerzita Karlova v Praze má právo na uzavření licenční smlouvy o užití této práce jako školního díla podle §60 odst. 1 autorského zákona.

V Praze dne podpis

Abstrakt/Abstract

Práce podává komplexní rozbor pohybu půdy buzeného seismickým vlnovým polem, zahrnující aspekty teoretické, geologické a geotechnické, jakož i analýzu dat a numerické simulace. Cílem je kvantifikovat hlavní parametry, umožňující odhad kmitavých pohybů v městských oblastech a případné snižování následků budoucích zemětřesení. Studie je zaměřena na Řím vzhledem k vysoké hustotě obyvatelstva a koncentraci historických památek s vysokou seismickou zranitelností. Práce zlepšuje údaje o podrobné povrchové geologii studované části Říma, vyplňuje mezeru ve znalostech geotechnických parametrů a poskytuje dosud chybějící záznamy zemětřesení na území města. Mimo jiné též umožňuje lépe pochopit prostorové rozložení škod, pozorované v Římě při dřívějších zemětřeseních. Hlavními inovacemi jsou: zřízení a dlouhodobý provoz seismické ereje, analýza seismického šumu a záznamy zemětřesné sekvence L'Aquila 2009. Trojrozměrná erej (zahrnující senzor v 70-m hlubokém vrtu) je první svého druhu v Itálii, která zaznamenala významné zemětřesení v městské oblasti. Pořízená instrumentální data jsou také porovnána s hybridní simulací pohybů půdy v údolí Tibery; jsou použity nové paralelizované programy, založené na metodě diskrétních vlnových čísel a 3D metodě konečných diferencí.

A comprehensive study of the soil shaking under the seismic wave-field excitation is presented. It includes theoretical, geological, geotechnical, data analysis and numerical simulations aspects. The aim is to quantify the main parameters allowing the estimate of the soil shaking in urban areas for better mitigating seismic risk due to future earthquakes. The city of Rome has been chosen as a case study because of its high density of population and large concentration of historical monuments with high earthquake vulnerability. This study improves significantly the knowledge concerning the detailed near-surface geology of the chosen study area of Rome, fulfills the absence both of knowledge concerning its geotechnical properties and earthquake data recordings in the city. Among others, it allows for a better explanation of the spatial damage pattern observed in the city due to earthquakes in the past. The main innovations include the construction and long-term operation a seismic array in the city, analysis of the natural seismic noise, and instrumental recordings of the 2009 L'Aquila earthquake sequence. The 3D array (including a borehole sensor at 70-m depth) is the first one in Italy planned, realized and operated within an urban area, and the first one that recorded a significant earthquake in the city. Finally, the recorded data are compared with hybrid numerical simulations of the ground motion in the Tiber valley, using new parallelized codes, based on the discrete-wave-number and 3D finite-difference methods.

Introduction

The damage produced during moderate and large earthquakes is significantly influenced, by the interaction between seismic waves propagation and near-surface geology of the site under study. Thus, the dynamical features of the soil shaking has been a matter of growing interest in seismological investigations, mainly at locations with high building vulnerability.

Studies concerning the so-called site effects analyze ability of the site to amplify the soil shaking in the range of frequencies of engineering interest, typically 0.2-10 Hz, ability to focus/defocus soil shaking in different parts of the site, etc. Naturally, the main interest is in expected ground motions of future strong earthquakes and understanding effects of past strong earthquakes. However, studies of the site effects can be also based on many other data, e.g.: (i) direct measurements of the site response using recordings of strong and weak earthquakes, in particular using specific arrays of stations (Chapter 2 of the present Thesis), (ii) measurement of the near-surface geology parameters and numerical simulation of the aforementioned seismic wave/near-surface geology interaction (Chapter 3), (iii) analysis of the so called seismic noise or ambient vibration (Chapter 1 and 2). The seismic noise is soil shaking in absence of earthquakes, in other words, it is the background signal and, as shown in the next paragraphs, huge information concerning the features of the soil shaking is hidden in it. The main goal of Chapters 1 and 2 is to illustrate how to extract from the seismic noise information relevant for site effect studies.

Whatever will be the adopted approach for studying site effects, knowledge about both the near-surface geology and geotechnical properties of the different lithologies is necessary. Such knowledge can be achieved by drilling boreholes for studying stratigraphy, performing geotechnical measurements such as down-holes and/or laboratory tests on undisturbed samples picked up at different depths and/or penetrometric tests, as well as using geophysical prospection, for example active seismic experiments. The physical quantity relevant for site effects is the vertical S-wave velocity (Vs) profile of near-surface geology. Integration of the information from the individual methods to characterize a site is schematically shown in Fig. 1. In this Thesis, studies about the near-surface geology are performed mainly for the Tiber valley in Rome, see Papers **P3** and **P4**.

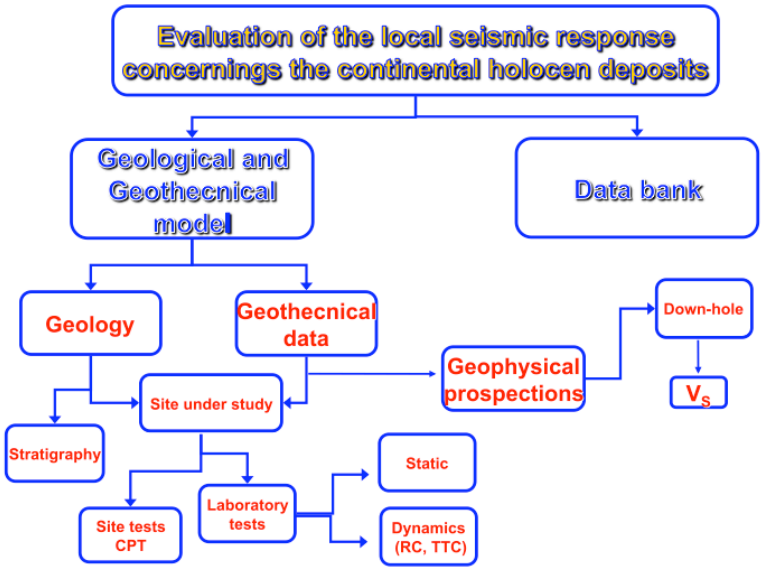

Figure 1: *Logical scheme of different approaches used in paper* **P3** *and* **P4** *for achieving geological and geotechnical information concerning concerning the site under study. From paper* **P3**.

Even though active seismic experiments and geotechnical information obtained from boreholes, complemented by the site and laboratory tests, provide a high quality information about the shallow subsurface structure, their cost is high and within densely populated urban environments, usually regions of high vulnerability, sometimes not even feasible. Moreover, they provide punctual information that must be generalized to the whole studied site, or a broader urban area.

On the other hand, since early work in the 1950's by Japanese seismologists (e.g. Aki (1957)), the use of passive, non destructive, seismological investigation of the shallow subsurface structure has been considered as a low-cost alternative to active seismic investigation methods, especially in urban environments. Such investigation is based on the analysis of aforementioned ambient vibration. In the present Thesis the seismic noise has been analyzed from deterministic and stochastic point of view; the former describes the dynamical process of interaction between the seismic waves and the near-surface geology (in terms of the wave propagation phenomena) while the latter describes the statistical features of the same process. Papers **P1** and **P2** deal with the stochastic side of ambient vibration, while papers **P3** and **P4** deal also with its deterministic side in view of generalizing the punctual information obtained by geotechnical investigation complemented by site and laboratory tests. The noise analysis is thus utilized in this Thesis

not only to obtain structural information about the near-surface layers, but also to proof, indirectly, the validity of the dynamic parameters extrapolation for the whole site of interest: the Tiber valley as case study.

In studying site effects the so called *experimental approach* can not be disregarded, i.e., an approach devoted to collect data of the local and regional seismicity of the area under study. That is why the realization of an array of seismic stations has been planned and realized under two multidisciplinary projects; in the first one the author of the present thesis has been the scientific responsible for the Research Unit 3, whereas in the second one he has been scientific responsible for the I.N.G.V. Chapter 3 is devoted to show the analysis of data collected by such array and their relevance for the seismic hazard in the city.

The interaction between elastic energy radiated from earthquake source and geological structures along the path up to the Earth surface can be modelled in detail using supercomputers. The irregularities of the geometry of geological layers and the presence of three-dimensional heterogeneities in the upper crust requires sophisticated computational techniques.

Numerical simulations of seismic wave propagation in heterogeneous media can be particularly useful when addressed to the assessment of the seismic response of the uppermost layers (a hundred meters beneath the surface) where seismic impedance shows a strong contrast between the rock basement and the softer sedimentary deposits of natural and anthropic origin. In these cases, the irregular geometry of the interfaces and the impedance contrast can cause trapping of energy and wave interference, resulting in large spatial variations of ground shaking at the Earth surface during earthquakes. These variations can be as large as a factor of 10 in specific frequency bands, within sites less than a hundred meters apart.

These effects attract a special attention in the urban areas where a systematic tendency to larger damage concentration has been experienced on outcrops of recent and unconsolidated terrains. In the last decades, an increasing number of seismic recordings has been available for many urban areas struck by strong earthquakes. Experimental data have allowed seismologists to understand the role of near-surface geology on the strength of shaking, explaining the mechanisms that cause the observed damage anomalies.

In addition to pure research purposes, this type of studies can have important implications for the seismic risk mitigation especially in urban areas where it would be better to know the soil shaking features before an earthquake occurs. The more suited tool for such purpose is represented by numerical simulations of the soil shaking. The Chapter 4 is devoted to numerically reproduce some spectral features observed in data analysis of Chapter 3, for the city of Rome. This has been done using data recorded by the installed roman array, concerning the April 6th 2009 Mw 6.1 earthquake occurred near the town of L'Aquila, 100 Km northeast of Rome.

Chapter 1

Seismic noise deterministic analysis: single station measurements

In seismology the ambient vibration is studied to achieve information on both the near-surface geology as well as the inner Earth structure. While the former concerns site effect studies mainly oriented for seismic hazard assessment and engineering seismology purposes (see Bard (1998) and Bonnefoy-Claudet et al. (2006)) the latter is more oriented to get information on the structure of the Earth's crust and upper mantle (Shapiro and Campillo (2004)). The two afore-mentioned topics usually investigate the seismic noise-field features in two different frequency ranges: 1 to 15 Hz for site effects and $5 \cdot 10^{-3}$ to 1 Hz for crust and upper mantle images. As far as the physical origin of the noise-field in such two ranges of frequencies concerns, it is widely accepted that the former range, called also microtremors, is basically linked with human activities, while the latter, called also microseisms, is due to natural processes such as ocean waves, tides, wind, etc. (Bard (1998)).

It must be said that the threshold f_{nh} of the order of 0.5 to 1.0 Hz has been conventionally chosen as the border between the two topics although they might have an overlap. Sometimes both engineering seismology is interested in frequencies lower than 1 Hz, and sometimes crustal studies involve the shallow geological layers as part of the Earth crust.

However, whatever will be the frequency range of interest one of the main problems is the interpretation of the results. It is intimately related to the composition of the seismic noise-field from different kinds of seismic waves, which in turn is dependent both on the sources of these vibrations, and on the underground structure. The present section will briefly summarize the present status of knowledge as far as those aspects necessary for the Thesis is concerned, whereas see Bonnefoy-Claudet et al. (2006) and

references therein; SESAME deliverable D13.08 for a comprehensive review, http://sesame-fp5.obs.ujf-grenoble.fr/SES_TechnicalDoc.htm, for a detailed discussion.

Understanding the physical nature and composition of the ambient seismic noise wave-field, especially in urban areas, requires answering two sets of questions, which are not independent of each other. Before starting such discussion it is worth noticing that beyond the scientific interest, answering these questions is important for better plan and realize technical methods for recording and interpreting the results. In other words, the answers to such questions affect applications of the noise methods and the interpretation of the results, that is why even though this is not the topic of the preset Thesis it will be briefly discussed. The two sets of questions are the following:

- what is the origin of the ambient vibrations (where and what are the sources);
- what is the nature of the corresponding waves, i.e., body or surface waves;
- what is the ratio of body and surface waves in the seismic noise wave-field;
- within surface waves, what is the ratio of Rayleigh and Love waves;
- again within surface waves, what is the ratio of fundamental mode and higher modes.

There is a relative consensus on the first two, in fact answers to the first question were given at the beginning of this paragraph whereas about the nature of the noise-field, Lachet and Bard (1994); Campillo and Paul (2003); Shapiro and Campillo (2004); Wathelet et al. (2005), (among others) have shown that the ambient vibration field is composed also by surface waves (Rayleigh and Love waves) in both frequency ranges (i.e., microtremors and microseisms). On the contrary, only few and partial answers were proposed for the remainder questions (strongly related to the site structure), for which a lot of experimental and theoretical work still lies ahead.

Besides this, only very little information is available on the quantitative proportions between body and surface waves, and within the different kinds of surface waves that may exist (Rayleigh/Love, fundamental/higher). The few available results, reviewed in Bonnefoy-Claudet et al. (2006), report that low frequency microseisms $f < f_{nh}$) predominantly consist of fundamental mode Rayleigh waves, while there is no real consensus for higher frequencies ($f > f_{nh}$). Different approaches were followed to reach these results, including analysis of seismic noise amplitude at depth and array analysis to measure the phase velocity.

	Natural	Human
Name	Microseism	Microtremor
Frequency	0.1 - f_{nh} (0.5 - 1 Hz	f_{nh} (0.5- 1 Hz) ¿ 10 Hz
Origin	Ocean	traffic/Industry/Human Activity
Incident Wave-field	Surface waves	Surface + Body waves
Amplitude Variability	Related to Ocean Storms Incident wave-field	Day-Night, Week-week-end Comparable amplitude-
Rayleigh/Love	predominantly Rayleigh	slight indication that Love waves carry a little more energy
Fundamental -Higer Modes	mainly Fundamental	Possibly of higher modes at high frequencies
Comments	Local wave-field may be different from incident wave-field	Some monochromatic waves related to machines and engines

Table 1.1: *Remarks summarizing the status of the art concerning the present knowledge on the nature and composition of the noise-field (from deliverable D23.12 WP12 of the SESAME project).*

The very few investigations on the relative proportion of Rayleigh and Love waves all agree on more or less comparable amplitudes, with a slight trend towards a slightly higher energy carried by Love waves (around 60% - 40%). In addition, there are a few reports about the presence of higher surface wave modes from several very different sites (some very shallow, other much thicker, some other with low velocity zone at depth). In Tab. 1.1 is summarized the present knowledge on the open question about both the physical nature of the noise-field and its compositions in terms of wave-types.

Because the main topic of the Thesis concerns studies related to site effects, attention is paid to microtremors. In this respect, the main target is how to retrieve the Vs vertical velocity profile from microtremors analysis only, fully disregarding information concerning the structure of the Earth's crust and upper mantle present in the noise field at low frequencies (micro-seisms).

1.1 H/V spectral ratio

As shown in the previous paragraphs, different approaches can be adopted to evaluate local site effects. Among the empirical low-cost methods involving seismic noise, the H/V spectral ratio on ambient vibrations is probably one of the most common one; the method, also called Nakamura technique (Nakamura (1989)), was first introduced by Nogoshi and Igarashi (1971) based on the initial studies of Kanay and Tanaka (1961).

The H/V method is an experimental technique to evaluate some characteristics of soft-sedimentary soils. It is based on the analysis of the spectral ratio between the Fourier amplitude spectrum of horizontal (H) components of the recorded ambient vibration, and the Fourier amplitude spectrum of the vertical component (V) of the same record.

Following the recommendations suggested in the deliverable D23 HV (http://sesame-fp5.obs.ujf-grenoble.fr/SES_TechnicalDoc.htm) of the SESA-

ME project, the first step in computing H/V spectral ratios is to divide the time series of each component in windows. The objective is to select and retain the most stationary parts of the ambient vibration excluding transients usually associated with specific sources such as footsteps and close traffic, just to name two. This is the opposite of what is done in seismology where detecting and tracking unusual transients is the main goal. Outlined here is a short description of the H/V technique.

For each selected window, the time series of each component is smoothed using a filter. SESAME suggests avoiding constant bandwidth smoothing because is not suitable for low frequencies, on the contrary, the Konno & Ohmachi smoothing is recommended as it accounts for the different number of points at low frequencies. We recall here that what low and high frequency means for ambient vibration has been clarified in the previous paragraph discussing the nature of the seismic noise field.

The two smoothed horizontal components can now be merged in different ways, SESAME recommends using the geometric mean. Next step is to compute the H/V spectral ratio with the merged H components. This has to be done for each selected time window. The obtained spectral ratios are averaged and standard deviation estimates are computed. Detailed discussion can be found in the SESAME deliverable D23 HV (http://sesame-fp5.obs.ujf-grenoble.fr/SE_TechnicalDoc.htm).

The findings summarized in Tab. 1.1, although partial, clearly demonstrate that the seismic noise wave-field is indeed complex, especially at high frequencies. In particular it implies, in interpreting the H/V ratio, that one has to consider the possible contributions to H/V from both surface and body waves, including also higher modes of surface waves; this will be the topic of the next two paragraphs.

1.1.1 H/V spectral ratio and body waves

The main question to address here is the relation of the H/V ratio, from the noise measurements, and site conditions for body waves; a side question concerns the differences or similarities between H/V ratios derived from earthquake recordings and H/V ratios derived from ambient vibration recordings.

When considering, on theoretical ground, a simple case represented by (at least) one soft layer over a half-space, and its response to obliquely incident plane waves, a striking result is the fact that, whatever is the incident wave type (P or SV or SH), the horizontal components systematically exhibit resonant peaks at the S-wave resonance frequencies, even for P wave incidence, while the vertical component always exhibit resonant peaks at the P-wave resonance frequencies, even for S wave incidence. This result is valid when the impedance contrast is large both for S and P waves, and comes from the conversion from P and SV waves at the bedrock/layer interface, and their relatively small incidence angles within the surface lower velocity layer

(see SESAME deliverable D13.08 and references therein, (http://sesame-fp5.obs.ujf-grenoble.fr/SES_TechnicalDoc.htm). On practical ground, the relation between H/V peak(s) and the S-wave resonance frequency is the following:

- the fundamental frequency is only weakly dependent on details of the structure of the near-surface geology; as a consequence the H/V ratio for a body wave-field should always exhibit a peak around the fundamental S-wave frequency, for high impedance contrast sites.

- in the case of horizontally stratified media, the H/V ratio should also exhibit peaks at the S-wave harmonics, at least for all peaks that do not coincide with a lower order harmonic of P-wave resonance.

- for horizontally stratified media with high impedance contrast, the amplitude of the first H/V peak is also expected to be somewhat correlated with the S wave amplification.

The above findings exhibit a few consistent, robust characteristics that have to be considered when interpreting experimental H/V peaks from recordings of seismic noise. First of all, the results are clear and simple in case of horizontally layered structures with large impedance contrasts ($>$ 4 – 5), while become more and more fuzzy for decreasing contrasts and for increasing underground interface slopes even for simple 1D geometry. Gathering the available geological and geotechnical information represents a big help in interpreting H/V peaks, in particular estimations of impedance contrasts are important because they are generally associated with either very young unconsolidated deposits, or very hard bedrock.

The link between H/V and the surface structure is then given by the standard 1-layer approximation represented by the rule of the quarter of the wave-length, i.e., $f_o = \frac{Vs}{4h}$ where f_o and Vs are the resonance frequency and the velocity of the S-wave, respectively, whereas h is the thickness of the layer.

Besides the use of H/V peak for obtaining info about Vs and/or the layer thickness, it is important to note its relation with the first frequency at which earthquake ground motion is amplified. Indeed, the H/V frequency peak represents the frequency value at which the soil shaking is amplified during earthquakes. This aspect is discussed in papers **P3** and **P4**, and it is confirmed by the data analysis of L'Aquila earthquake as felt in the city of Rome in Chapter 4.

The last aspect is the main difference from the surface wave part of the noise case, where it is not generally expected any correlation between H/V spectral peaks and the actual amplification of the soil shaking due to earthquakes. Whereas the amplitude of H/V peaks has no relation with the

actual amplification of the soil shaking at the same frequency neither for body waves nor for surface waves.

1.2 Seismic noise deterministic analysis: array measurements

Bides the widely used single-station analysis method known as H/V ratio or Nakamura's method previously discussed, the use of small-aperture arrays allows to derive frequency dependent estimates of the phase velocity of the noise wave field. The dispersion curve information can be used to derive velocity models for a given site in an inversion as well as in a forward procedure.

The use of these methods have become wide-spread in recent times (Horike (1985, 1996); Ishida et al. (1998); Miyakoshi et al. (1998); Yamanaka et al. (1994); Sherbaum et al. (2003)), it happened particularly in Japan (Tokimatsu (1997); Chouet et al. (1998); Bettig et al. (2003); Satoh et al. (2001); Wasten and Dhu (1998)).

Given the assumptions, according to what has been discussed in the previous paragraph, that the site structure is horizontally stratified (1D approximation) and ambient vibration is predominantly made of surface waves, array measurement analysis allows retrieving the dispersion curves of surface waves Tokimatsu (1997). Major advantages of these techniques are that they can be applied in urban areas and that they are able to investigate deep soil properties, up to 1/3 of the wave-length corresponding to the fundamental resonance mode (see pervious paragraph), according to the low frequency content of the seismic noise (Horike (1985); Ishida et al. (1998); Miyakoshi et al. (1998); Yamamoto (2000); Sherbaum et al. (2003)). These two features are of particular interest in site effect assessment, as numerous big cities in seismic areas (Mexico City, Los Angeles, Caracas, Tokyo, etc.) are built on thick soil layers (from hundreds meters to more than 1 Km depth).

Our purpose is to reconstruct from array measurements of ambient vibration, the dispersion curve of the Rayleigh waves. This can be done via an inverse or forward problem, in the present Thesis the forward problem has been solved. In practice, a comparison between the dispersion curve obtained by ambient vibration recordings and the dispersion curve obtained by a 1D model of stratified surface soil has been performed, the stratification represents the vertical Vs profile of the near-surface geology, i.e., our final target. Such technique has been applied first in the site where geological and geotechnical investigations were previously performed with the purpose of better tuning the technique (Fig. 1.1 top).

Later, the same tuned procedure has been applied in other sites within the Tiber valley (Fig. 1.1 middle and bottom rows), in order to geneneralize

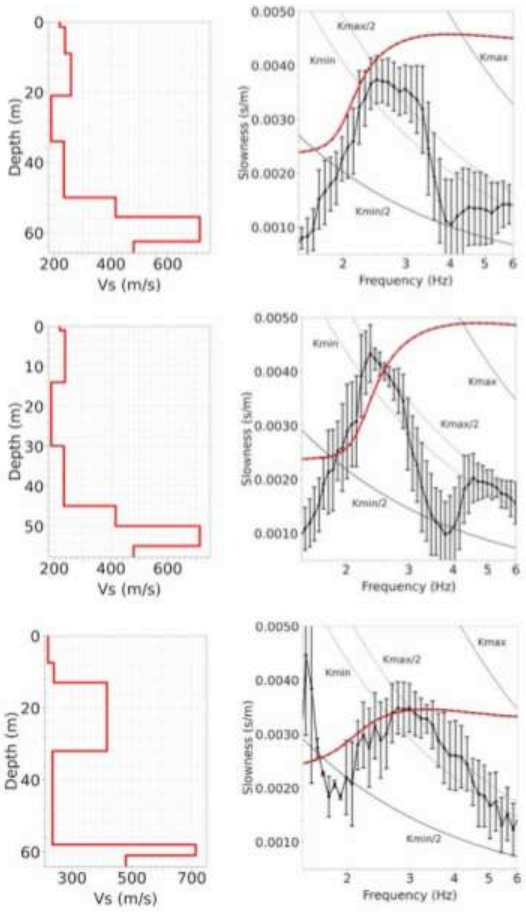

Figure 1.1: *Columns from the left: Vs vertical velocity profiles; theoretical dispersion curves (solid red lines) computed using Vs and experimental dispersion curves (stippled black line), the vertical bars are ±1 standard deviation. Row from top: test site, the two sites within the Tiber valley. From paper* **P3**.

the results concerning the Vs vertical profile to whole sedimentary body of the city (see paper **P3**). The same procedure has been applied to a tributary lateral valley (Grottaperfetta valley) of the main sedimentary body of the city (see paper **P4**). In the following paragraphs will be illustrated those aspects of the array measurements technique that are relevant in respect of the work done in the present Thesis, without intention of showing an exhaustive treatment of the whole topic. For detailed discussion refer to, among others Sherbaum et al. (2003); Ohrnberger et al. (2004a); Wathelet et al. (2005); technical documentation of SESAME project at http://sesame-fp5.obs.ujf-grenoble.fr/SES_TechnicalDOC.htm in particular the deliverable D24-Wp13.

1.2.1 Dispersion curve estimate

In order to allow a reliable determination of the vertical velocity structure itself Vs by any inversion as well as forward algorithm, a dispersion curve estimate of acceptable quality within a broad frequency range is required. Taking into account that ambient vibration is made mainly by Rayleigh waves in the vertical plane of motion whereas in the horizontal plane by both Rayleigh and Love waves, analyzing vertical components of the array records of the ambient vibration is enough to estimate the dispersion curve of the Rayleigh waves. So, we are interested in the vertical components only.

To estimate the dispersion curve of Rayleigh waves the first step is to install a 2D array of seismic stations. Problems related to the array geometry, its size and how both such aspects are linked with the frequency resolution and the frequency limits of validity of the estimation, will be discussed in details in the next paragraph. The second step is to estimate the dispersion curve of the Rayleigh waves from the vertical component of the seismic noise records. Such estimation can be done through different approaches. These latter can be divided into two groups: frequency wave-number techniques (F-K, after Kvaerna and Ringdahl (1986)) and spatial autocorrelation techniques (SPAC, after Aki (1957); Capon (1969)). As far as the ambient vibration analysis concerns, the former are based on both a time-delay measure and few noise sources, whereas the latter is based on both the measure of the spatial coherence of the steady waveforms and non-correlated sources randomly distributed in space and time (Bettig et al. (2003)). It is worth noticing that both the aforementioned methods are based on plane wave approximation of the seismic noise wave-field.

In the present Thesis has been adopted a particular F-K method called CVFK. It is a conventional semblance based frequency wave-number method after Kvaerna and Ringdahl (1986), evaluated in sliding time window manner and narrow frequency bands around some center frequency. The coher-

ence estimate is given by:

$$R\left(\omega, \overrightarrow{k}\right) = \frac{\sum_{m=1}^{M} \left| \sum_{n=1}^{N} X_n\left(\omega_m\right) e^{i\omega_m \overrightarrow{k} \cdot \overrightarrow{r_n}} \right|^2}{\sum_{m=1}^{M} \sum_{n=1}^{N} \left| X_n\left(\omega_m\right) e^{i\omega_m \overrightarrow{k} \cdot \overrightarrow{r_n}} \right|^2} \tag{1.1}$$

where $X_n\left(\omega_m\right)$ are the complex Fourier coefficients of the observed signal (vertical component) at station n, $(n = 1, 2, \cdots, N)$) and at discrete frequency ω_m, $(m = 1, 2, \cdots, M)$. The vector $\overrightarrow{r_n}$ represents the position in space, measured from a fixed origin, of the $n - th$ station. The phase shift $e^{i\omega_m \overrightarrow{k} \cdot \overrightarrow{r_n}}$ accounts for the delay times related to the horizontal wave-number $\overrightarrow{k}$ from which the direction θ, in the (k_x, k_y) plane, and the horizontal slowness s can be derived as

$$\theta = \arctan\left(\frac{k_y}{k_x}\right) \qquad s = \frac{\left|\overrightarrow{k}\right|}{\omega} \tag{1.2}$$

The coherence estimate 1.1 is called frequency-wavenumber power spectrum estimator, in literature more than one of such estimator functions can be found (for a detailed discussion refer to the SESAME deliverable Del-D24-Wp13; http://sesame-fp5.obs.ujf-grenoble.fr/SES_TechnicalDoc.htm). However, whatever will be the chosen estimator, its use for estimating dispersion curve of surface waves does not change. In fact, to obtain the propagation characteristics of the most coherent plane wave arrival, a grid search over the wave-number plane (k_x, k_y) is performed. A wave-number grid layout, which is sampled equidistantly in slowness and azimuth, is used.

The experimental dispersion curve can be used to retrieve Vs solving an inverse problem. On the contrary, in the present Thesis such experimental dispersion curve has been compared with the dispersion curve obtained tuning the Vs as it arose from geotechnical field investigations made in the test site within the Tiber valley (see **P3** and **P4**). Such tuned Vs has been then used to estimate Vs in the whole Tiber valley through a forward problem applied to the array analysis of the seismic noise records.

1.2.2 Array geometry, resolution and aliasing

An important issue in any array measurement is the question of optimal geometry (size, shape, number of sensors, etc.) regarding the resolution limits and spatial aliasing effects. This topic has been treated both for large aperture arrays in the context of earthquake/explosion monitoring (Haubrich (1968); Harjes (1990)) as well as in the field of small aperture array for ambient vibration processing (Woods and Lintz (1973); Asten and Henstridge (1984); Kind (2002)). The main differences between these different fields of application can be attributed to the signal components of interest that are to

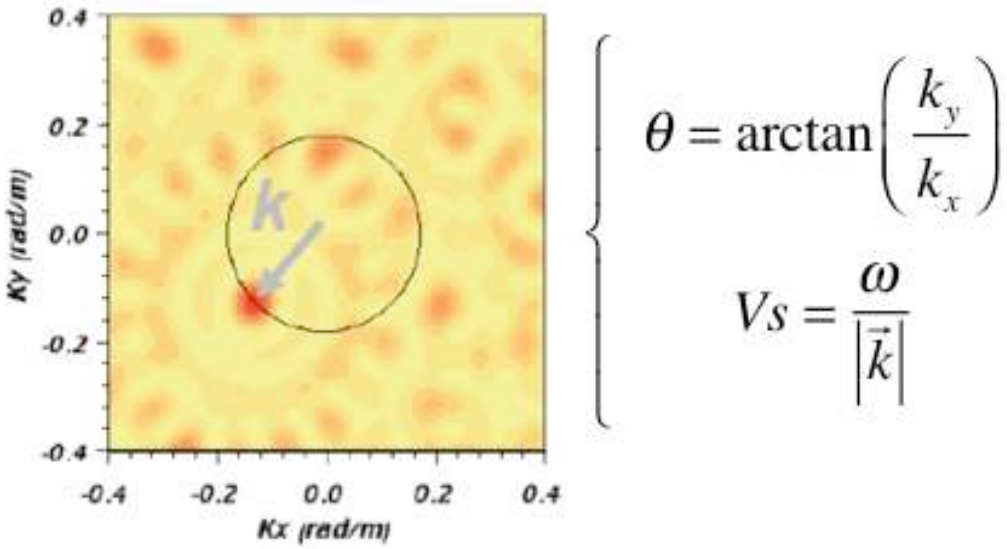

Figure 1.2: *Contouring of the coherence estimator function 1.1 in the plane* (k_x, k_y)*, at fixed frequency* ω*. Red spots are the relative maxima of the power spectrum estimator 1.1.*

be analyzed. Whereas in the field of earthquake detection, arrays are usually optimized for undispersed broadband transient signal arrivals (body wave detection) from relatively distant sources (plane wave-front), for ambient vibration surveys we have to consider a mostly random wave-field caused by nearby superficial sources which has to be analyzed within narrow frequency bands.

Due to the aim of investigation, i.e., the determination of frequency dependent phase velocity curves, array methods have to be employed for a narrowband analysis of the ambient vibration wave-field. Compared to broadband processing, the resolution of narrowband array responses is significantly reduced and aliasing peaks are fully developed (Kind (2002); SESAME deliverable no. D24 Wp13 http://sesame-fp5.obs.ujf-grenoble.-fr/SES_TechnicalDoc.htm).

Unfortunately, the use of broader frequency bands is prohibitive for the determination of dispersion characteristics (Wathelet et al. (2008)). Thus, an enhancement of the resolution/aliasing capabilities for narrowband analysis can only be achieved by improving the spatial sampling of the wave-field. In turn, this requires the use of a large number of stations in field experiments. Clearly, viewed from the economical perspective, this option is prohibitive in most cases considering the initial equipment cost, the increased logistical effort and additional man power required for field exper-

iments. Given the economical and logistical constraints, there is little one can do with respect to the resolution/aliasing issue for dispersion curves, except choosing an appropriate array size and array geometry, suitable for the analysis of a narrow wavelength range.

Unfortunately, at the present time there is no global agreement about the capabilities of an array designed at recording ambient vibrations. Asten and Henstridge (1984) recommended that the array diameter should be at least as large as the longest wavelength of interest and that the station spacing for any direction should be less than half the shortest wave-length of interest so as to avoid aliasing in the wave-number domain. Asten and Henstridge (1984) proposed the following relationships between the minimum and maximum sensor spacing (D_{min} and D_{max}) and the minimum and maximum wave-lengths (λ_{min} and λ_{max}) necessary to achieve reasonable results

$$\begin{cases} \lambda_{max} = 3D_{max} \\ \lambda_{min} = 2D_{min} \end{cases} \tag{1.3}$$

First relation comes from active source methods for linear arrays and it allows reasonable results to be obtained for ambient vibration arrays as well Tokimatsu (1997). The second one is derived theoretically from Nyquist wave-number. Considering a penetration of the order of half λ_{max} (Xia et al. (2000)) for surface waves, the maximum depth for which Vs can be computed is about 1.5 D_{max}.. Accordingly, Satoh et al. (2001) proposed the maximum wave-length to be two to four times the maximum sensor separation. Gaffet (1998) stressed out that the λ_{min} limit obtained from the minimum sensor spacing is not well adapted to an irregular array grid, as a minimum of 2 points per wavelength is not guaranteed over the entire array. More recently, Kind et al. (2005) used the common rules of thumb to quantify the low frequency limit of the deduced dispersion curve, and a manual interpretation to identify the aliasing limits. In terms of wave-number, the dimensions of the array can be expressed as (Scherbaum (1996); Tokimatsu (1997))

$$\begin{cases} k_{min} = \dfrac{2\pi}{D_{max}} \\ k_{max} = \dfrac{2\pi}{D_{min}} \end{cases} \tag{1.4}$$

the dispersion curve obtained from array processing is considered to be reliable within these two boundaries; this holds for every processing technique and defines a limit over which spatial aliasing is very likely to occur. The actual numerical values of k_{min} and k_{max} depend not only on the array size but also on its geometry. An estimate can be done, on theoretical ground, using the so called array transfer function or theoretical beam pattern. This is the topic of the next paragraph.

1.2.3 Array transfer function

On theoretical ground the performance of a given array geometry is evaluated by the array response pattern, also known as theoretical array transfer function or theoretical beam pattern (R_{th}), commonly depicted for a vertically incident plane wave. This because after Woods and Lintz (1973), the resolving power of an array depends not only on the diameter of the array but also on the spatial distribution of the sensors and on the correlation between the events to be resolved. They proposed to estimate this resolving power by using the theoretical array response function (R_{th}). This latter function is given in the (K_x, K_y) plane by (Woods and Lintz (1973); Asten and Henstridge (1984))

$$R_{th}\left(K_x, K_y\right) = \frac{1}{n^2}\left|\sum_{j=1}^{n} e^{-i(K_x x_j + K_y y_j)}\right|^2 \tag{1.5}$$

where n is the number of sensors in the array, and (x_j, y_j) are their coordinates.

For one single plane wave $S_j(f) = A(f)e^{i\left(x_j K_x^1 + y_j K_y^1 - 2\pi f t + \phi\right)}$ crossing the array at wave-number $\left(K_x^1, K_y^1\right)$ recorded at sensor j with a phasei ϕ, the array output is

$$\begin{aligned} R_{th}\left(K_x, K_y, f\right) &= \left|\sum_{j=1}^{n} S_j(f) e^{-i(K_x x_j + K_y y_j)}\right|^2 \\ &= n^2 A^2(f) R_{th}\left(K_x - k_x^1, K_y - K_y^1\right) \end{aligned} \tag{1.6}$$

where $A(F)$ is the amplitude spectrum. The array output 1.6 is equal to the theoretical response 1.5 translated by a vector $\left(K_x^1, K_y^1\right)$ and multiplied by the square of the amplitude.

For multiple plane waves travelling across the array, $S^{(1)}$ to $S^{(m)}$, the array output is

$$\begin{aligned} R_{th}\left(K_x, K_y, f\right) &= \left|\sum_{j=1}^{n}\sum_{l=1}^{m} S_j^{(l)}(f) e^{-i(k_x x_j + K - y y_j)}\right|^2 \\ &\leq n^2 \sum_{l=1}^{m} R_{th}^{(l)}\left(K_x, K_y, f\right) \end{aligned} \tag{1.7}$$

where $R_{th}^{(l)}$ is the array output for the single plane wave l defined by equation 1.6, and $S_j^{(l)}$ the wave l recorded at station j. In this case, the array output is always lower than the sum of translated theoretical responses, and it cannot be simply interpreted as the summation of the individual shifted theoretical array responses (Wathelet et al. (2008)). From equation 1.5, the theoretical

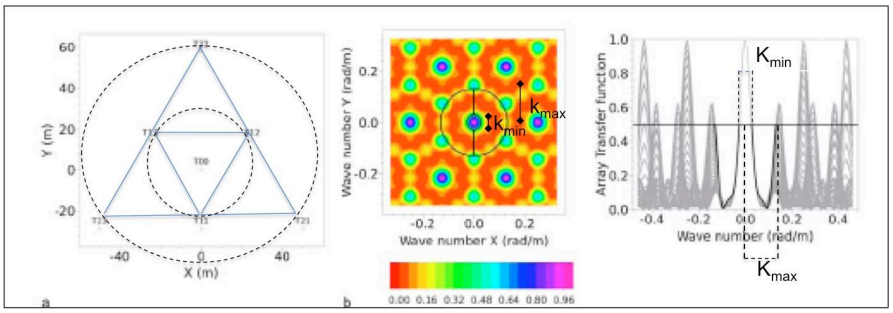

Figure 1.3: *left panel: array geometry; middle panel: contouring of the theoretical beam pattern* (R_{th}) *corresponding to the array geometry plotted in the left panel; black circles in the* (K_x, K_y) *plane show the alias-lobe positions,* K_{min} *and* K_{max} *represent their radii. Right panel: vertical section of the* (K_x, K_y) *plane in the azimuth represented by the black bold line in the middle panel; black bold curve represents where* (R_{th}) *magnitude reaches the value of 0.5* (K_{max}) *along such azimuth. Redrawn from paper* **P3**.

response R_{th} always exhibits a central peak (Fig. 1.3) which value is one (K_x and $K_y = 0$) and secondary aliasing peaks which amplitude are less or equal to one. Equation 1.6 shows that the position of the highest peak of the real array output is directly linked to the apparent velocity and the azimuth of the propagating wave. For a simple wave-field (equation 1.6), aliasing occurs for all wave-numbers greater than half the wave-number of lateral peaks of R_{th} which reach a value of 1 (Fig. 1.3 middle panel). For a complex wave-field (equation 1.7), aliasing is likely to occur at wave-numbers lower than this value, due to the summation of secondary peaks of R_{th}.

Concerning the resolving power, the thinner is the central peak of R_{th}, the more capable is the array to distinguish two waves travelling at close wave-numbers (Asten and Henstridge (1984)). Resolution and aliasing limits are then directly derived from the R_{th} map. Following Woods and Lintz (1973), the resolution limit ($K_{min}/2$) is taken as the radius of the central peak of R_{th} measured at the mid-height (0.5). We dene the aliasing limit (K_{max}) as the lowest K value (greater than $K_{min}/2$) obtained at the intersection of R_{th} with the horizontal line at 0.5, considering all directions (Fig. 1.3 right panel). These two limits are illustrated in the middle panel of Fig. 1.3 by black circles while the bold black curve in the right panel corresponds to the azimuth with the most restrictive limit. For simple and regular array geometries, $K_{min}/2$ and K_{max} can be linked to the maximum and minimum distances between sensors through relations 1.3. For irregular and more usual arrays, these limits are dependent on the spatial distribution of sensors and can be more rigorously defined from the theoretical array response.

1.3 Conclusive remarks

To summarize the main points for getting quality array measurements and processing when ambient vibration is used, let first note that whatever will be the processing method adopted (F-K or SPAC) it assumes that the investigated site is made of horizontal layers with velocity values varying with depth. Before any deployment of a seismic array, the one-dimensional structure of the site has to be assessed from existing geological data and/or from the spatial stability of the H/V curves.

No simple relation between the array geometry, the penetration depth and the usable frequency range of the dispersion curve is available in literature. To address this problem, one has to compute the theoretical array response which yields two wave number limits (K_{min} linked to array resolution, K_{max} linked to array aliasing) defining a validity range for the estimated dispersion curve. Tests on synthetic signals have shown that the dispersion curve estimations from both F-K and SPAC methods are reliable within this wave number range (Bonnefoy-Claudet et al. (2004); Cornou et al. (2004); Ohrnberger et al. (2004a,b); Wathelet et al. (2008)). Interpretation of results outside these limits is in general not recommended.

The array performance is controlled by several factors, one of them is the slowness resolution. It is linked with the inverse of the main lobe width of the beam pattern R_{th} function. So that the smaller is the width of the main lobe and the higher will be the slowness resolution. On the other hand we have seen in the previous paragraph that such width is K_{min} linked with the array aperture, D_{max}, through relation 1.4. So, we can conclude that the more the array aperture is bigger the higher will be the slowness resolution.

Another factor is the main lobe/side lobe distance of the R_{th} function, we have seen in the previous paragraph that it is represented by K_{max}. This latter is inversely proportional to the shorter station distance D_{min} through relation 1.4. So we can conclude that the shorter is D_{min}, the bigger isK_{max} that is, the longer will be the main lobe/side lobe distance. This means that farer, in terms of wave-number, the aliasing effects will take place. In other words, larger will be the frequency band available for being investigated by the array.

Fig. 1.4 summarizes these results showing the role played by the array geometry, with fixed number of stations, in determining the K_{min} and K_{max} values. Starting from the top-line, is well visible how K_{max} decreases as the array aperture increases. At the same time, the slowness resolution increases as the array aperture increases.

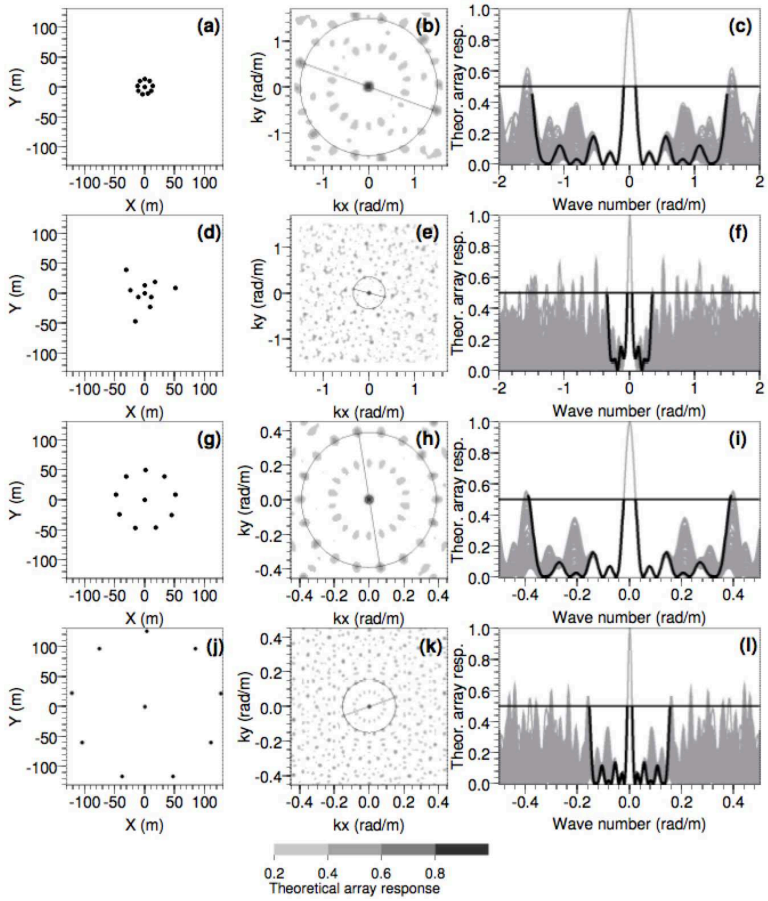

Figure 1.4: *Array geometries are in first column, their corresponding theoretical frequency-wavenumber response is in the second column. The circles correspond to the chosen wave-number limits. Black curves in the third column correspond to the orientation of the diameters drawn in the second column. From Wathelet et al. (2008).*

Chapter 2

Seismic noise analysis: stochastic approach

Starting in the 1980s, a growing number of researchers understood the importance of studies concerning the non-linearities in Geophysics. So that they focused their efforts on such topic giving rice to the so called non linear Geophysics (NG). Many different phenomena show the same behaviors if they are seen from the non-linearities point of view. This experimental observation leaded the researchers to think of the existence of some fundamental lows, called *self-organization laws,* able to go beyond the linear description of the dynamics driving the systems behaviors, that at the best can describe small perturbations only, through the real nature of the observed dynamics.

NG can provide a rational basis and a theoretical unified frame for natural systems including hazards. The main NG improvement in respect of a pure deterministic description indeed, has been to import from theoretical Physics into Geophysics the use of the general concept of self-organized criticality (SOC). SOC relates the statistical features that are scale invariant, having in such a way a fractal nature, to the non-linear dynamics that has generated such statistical features in the systems behavior.

The simplest example is the forest fire trend, which gives a robust power law relation between the size (area) of forest fires and their frequency of occurrence. Despite its simplicity, this model simulates the frequency-area statistics of actual fires in nature much better than classical alternatives (Malamud et al. (1998)).

Similarly, SOC models indicate that the Gutenberg-Richter frequency-magnitude statistics for earthquakes are a combined effect of the geometrical (fractal) structure of the fault network and the nonlinear dynamics of seismicity. The application of NG methods is thus indispensable for extreme phenomena and new hazard assessment techniques (Rundle et al. (2003)).

According to this relatively recent geophysical mood, an attempt to in-

vestigate the physical information on the soil shaking features hidden in the seismic noise from NG point of view, has been included in the present Thesis. Such contribution can be divided into two papers, **P1** and **P2**, corresponding to the two adopted points of view: one based on numerical simulations aimed at reproducing physical behavior of some statistical quantity such as the decay of coherence versus distance of the wave propagation, and the other one based on data analysis of the actual ambient vibration records with the aim to investigate the scale invariant statistical properties characterizing seismic noise, if any.

Within the previous discussed site effects framework, the NG approach has been adopted with the target first to quantify the degree of heterogeneity of the analyzed soils, and later to relate such degree of heterogeneity with the soil conditions. This has been done first through the coherence analysis of synthetics signals (numerically simulated) of the Earth crust wave propagation up to the site under study (paper **P1**), and later going deeper through the statistical properties of the ambient vibration records by the fractal analysis (paper **P2**). Such NG aspects will be the topic of the next paragraphs.

2.1 Seismic noise stochastic analysis: coherence numerical simulation

The higher is the degree of the soil heterogeneity, the more the wave-field is scattered and the higher will be the loss of coherence as function of distance travelled by seismic waves. Thus, the loss of coherence is a good candidate to be investigated for quantifying the degree of soil heterogeneity.

From field observations arise two coherence features: seismic wave propagation becomes incoherent at a distance of one wave-length in rock-sites (M.N. Toksöz et al. (1991)) and the coherency level of the seismic wave propagation in large sedimentary basins is higher than in rock-sites (Schneider et al. (1992)). The former behavior is ascribed to the scattering that takes place along the propagation path within the Earth's crust (Menke et al. (1990); M.N. Toksöz et al. (1991)); the latter is attributed to the resonance properties of basins that make seismic wave propagation more coherent (Schneider et al. (1992); Hough and Field (1996)).

Both features arise from a wealth of fine structures in the Earth's crust, as well as in the near-surface geological structures that cannot be represented in a detailed enough manner for its behavior to be described in a deterministic way, that is why we decided to approach the problem from NG side. More in detail, we want to numerically reproduce such coherence behavior concerning both the crustal and basins propagation.

For that purpose we assume that the scattering effects on small-scale crustal heterogeneities can be represented as a perturbation, $\xi(t)$, to the

crustal deterministic wave propagation, $x(t)$, so that the seismic wave propagation through the Earth crust, $y(t)$, can be represented as

$$y(t) = x(t) + \xi(t). \tag{2.1}$$

In order to numerically quantify the degree of crustal $y(t)$ signal correlation, we think of $\xi(t)$ as a set $\{\xi_i(t)\}$ $i = 1, 2, \cdots, N$, of random time series ideally located along a source line in the numerical 2D computational domain. The $\xi_i(t)$ random time series are assumed to be stationary and with zero mean so that the expected value of the corresponding crustal seismic signals $y_i(t)$ will be equal to the deterministic components $x_i(t)$, i.e., $E\left(y_i(t)\right) = x_i(t)$. The cross-correlation function for the stationary stochastic process is defined as

$$R_{l,k}(\tau) = E\{[y_l(t) - x_l(t)][y_k(t+\tau) - x_k(t+\tau)]\} = E\{\xi_l(t)\xi_k(t+\tau)\} \tag{2.2}$$

In the frequency domain relation 2.2, for finite duration signals, becomes (Priestley (1981))

$$H_{l,k}(\omega) = \lim_{T\to\infty} E\left\{\frac{(\hat{\xi_l}(\omega))^* \hat{\xi_k}(\omega)}{T}\right\} \tag{2.3}$$

where $*$ stands for complex conjugate and the $\hat{\xi_k}(\omega)$ are the Fourier transforms of the random signals $\xi_k(t)$ over a time window T. In the end, the cross-spectrum $H_{l,k}(\omega)$ is the Fourier transform of $R_{l,k}(\tau)$ so that when $l = k$ the cross-spectrum provides the power spectral densities of the random signals $\xi_l(t)$. The degree of correlation between the stochastic time series $\xi_i(t)$ has been evaluated using the absolute value of the coherence defined as (Priestley (1981))

$$|W_{l,k}(\omega)| = \frac{|H_{l,k}(\omega)|}{\sqrt{H_{l,l}(\omega)H_{k,k}(\omega)}}.$$

As previously mentioned, the seismic radiation propagating in rock-site environments becomes incoherent over distances greater than one wave-length and the loss of spatial coherence with distance and frequency, can be represented by an exponential function (Menke et al. (1990); Hough and Field (1996); Riepl et al. (1997)). This leads us to choose the following functional form for the coherency decay

$$w_{l,k}(\lambda) = |W_{l,k}(\omega)| = \exp\Big(-\frac{d_{l,k}}{\delta(\lambda)}\Big) \qquad \text{where} \qquad \delta(\lambda) = -\frac{2\pi c}{\omega \ln(0.3)} \tag{2.4}$$

where c, λ and $d_{l,k}$ are the wave velocity, the wave-length and the constant spatial distant between the stochastic time series $\xi_l(t)$, respectively. That choice of $\delta(\lambda)$ in 2.4 represents a 70 % coherency decay after one wave-length.

From the above assumptions and equations, the absolute value of the cross-spectrum $H_{l,k}(\omega)$ can be represented, for a fixed frequency (or wavelength), by the following symmetric matrix

$$H = \begin{pmatrix} 1 & \Theta & \dots & \Theta^{N-2} & \Theta^{N-1} \\ \Theta & 1 & \dots & \Theta^{N-3} & \Theta^{N-2} \\ \vdots & \vdots & \ddots & \vdots & \vdots \\ \Theta^{N-2} & \Theta^{N-3} & \dots & 1 & \Theta \\ \Theta^{N-1} & \Theta^{N-2} & \dots & \Theta & 1 \end{pmatrix} \tag{2.5}$$

where $\Theta = \exp(-d_o/\delta(\lambda))$ and d_0 is the constant spacing between two consecutive stochastic time series $\xi_l(t)$. The matrix 2.5 and the relation 2.3 suggest estimating the N elements of the symmetric matrix 2.5 as

$$h_{|k-l|}(\omega) = \frac{1}{T} \left| \frac{\sum_{i=1}^{N-|k-l|} (\hat{\xi}_i(\omega))^* \hat{\xi_{i+n}}(\omega)}{N-n} \right| \tag{2.6}$$

with l and k indicating the rows and the columns of the matrix 2.5, respectively. The estimate 2.6 is based on the assumption that the spatial variation of the cross-spectrum for the stochastic signals can be represented by a function of the relative distances $d_{l,k}$ between the points on the source line in the 2D computational domain.

To summarize, we have to generate a set of N random time series $\{\xi_k(t)\}$ in such a way that their coherence behavior with distance can be estimated through 2.6. This latter has to fit with the theoretical behavior expressed in 2.4. Thus, the point is how to numerically generate such N random time series $\xi_k(t)$. In the paper **P1** is shown how the set $\{\xi_k(t)\}$ is generated using a Monte Carlo method based on a random walk in an *ad hoc* N-dimensional phase space.

Getting the set $\{\xi_k(t)\}$, through relation 2.1 the synthetic Earth crust propagation is available as input for numerically simulating the 2D site response. In paper **P1** is designed a numerical experiment to investigate how the coherence of the bedrock motion relates to the coherence of the surface ground motion in a sedimentary valley. In other words, the wave crustal propagation 2.1 has been used in seismology with the aim to improve the tuning of the stochastic component of the wave-field to agree with the assumed coherence low 2.4.

Has to be noted that the Monte Carlo method adopted in paper **P1** does not depend neither on the coherency decay law nor on the incoherence threshold over one wavelength, both given in expression 2.4; the method works with other decay laws as well.

2.2 Seismic noise stochastic analysis: a fractal approach

In respect of NG point of view, the paper **P1** represents the minimum expansion toward the stochastic side of a deterministic approach. In fact, the non-deterministic part of the wave propagation process, represented by the scattering, is seen as a perturbation (stochastic noise) to the pure deterministic crustal propagation.

Now we go deeper inside the stochastic nature of the ambient vibration; the aim is to study physical information hidden in the seismic noise and how such information can be related to the soil conditions. More in details, we are interested in 3D soil displacement vector to study the global soil motion under the effect of noise field. In Fig. 2.1 the different nature of the short time-scale 3D motion is shown for both firm and unconsolidated soils. The different roughness suggests different diffusive nature of the soil motion; we want to quantify such differences in roughness, to understand their physical and dynamical origins and how such differences are linked with soil conditions (near-surface heterogeneity). Such results are obtained in the paper **P2**, here we illustrate those aspects needed to better understand the theoretical framework from which the results of paper **P2** have been originated. In looking at Fig. 2.1 some questions arise

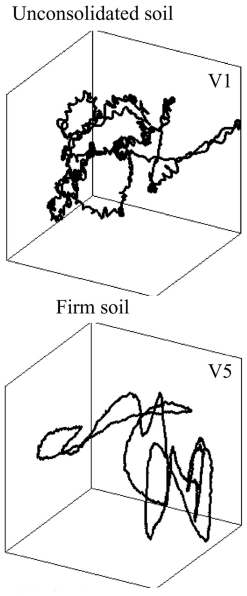

Figure 2.1: *3D soil displacement due to noise-field recorded on unconsolidated and firm soils, respectively.From paper* **P2**.

- differences in roughness are actually due to a diffusive process?
- in case, how long is the memory of such diffusive process?
- how to recognize statistical features in the time-history?
- are such statistical features invariant through different time-scales, i. e., what are their scaling properties (if any)?

To answer these questions let's start first from what we already know about both the Brownian motion and the white noise, and later let us investigate what relations link them, if any.

2.2.1 Brownian motion and white noise

The Brownian motion (Bm) can be thought as a time-dependent random variable $x(t)$ representing the position of the particle at time t that has the velocity ν. Its expected value is $E(x(t)) = 0$ and its standard deviation is $\sigma(t) \sim \sqrt{(t)}$. In the end we have that $x(t)$ follows a gaussian distribution with null expected value and a standard deviation that increases with time as the square root of t. As a consequence the scaling between time and space is not the same: if we rescale the time by a factor λ, we have to rescale the spatial coordinate by a factor $\sqrt{\lambda}$ in order to preserve the statistical properties of the process.

Such anisotropic scaling is illustrated in Fig. 2.2. In the top panel five different realizations of the same Bm are shown. The bottom left panel illustrates that Bm is not self-similar under isotropic spatial and temporal scaling. Indeed, the traces are not similar to the original ones. On the contrary, the bottom right panel shows an anisotropic rescaling according to the previously mentioned scaling properties of the Bm.

The traces in the anisotropically magnified section look similar to those in the top panel. This suggests *self-affine* scalar invariance, indicating this latter by definition (Sornette (2000)) objects which are statistically similar under anisotropic scaling.

A deep and strong link exists between Bm and diffusive processes (Sornette (2000)). The relationship $\sigma(t) \sim \sqrt{t}$, also called *root-t law* is ubiquitous in diffusive transport phenomena such as heat transport or spreading of pollutants in the ground, phenomena these latter generally described by classical diffusion equation.

Considering the velocities, $f(t)$, involved in Bm as statistical process in place of displacements, at different times they are just independent, Gaussian-distributed random variables. Thus the velocities represent a statistical process called *white noise* (Wn); using such description we need $x(t)$ any more. The statistical properties of $f(t)$ can be summarized in the form

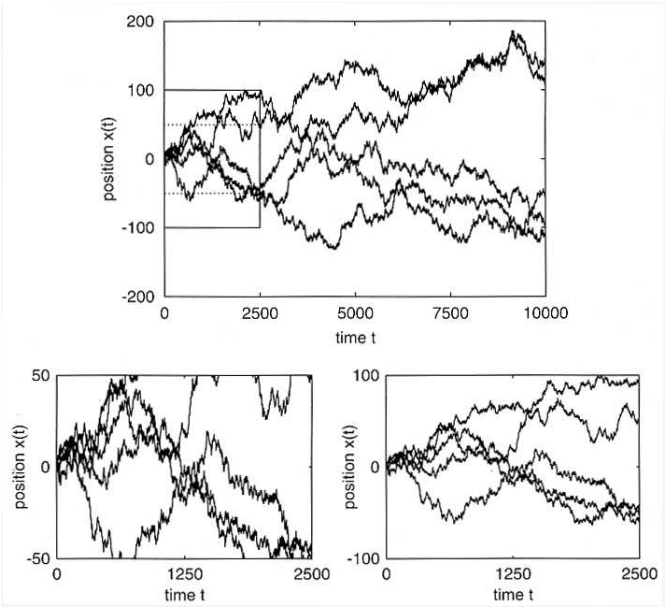

Figure 2.2: *five realizations of the same Brownian motion (top) and magnified sections (bottom). Bottom left: isotropic magnification (dashed section in the top panel); bottom right: anisotropic magnification (solid section in the top panel). Hergarten (2002).*

(Sornette (2000))

$$E\left(f(t)\right) = 0 \qquad \text{and} \qquad E\left(f(t)f(t')\right) = \begin{cases} \frac{c}{\delta t} & \text{if } \left[\frac{t}{\delta t}\right] = \left[\frac{t'}{\delta t}\right] \\ 0 & \text{else} \end{cases}$$

with (Sornette (2000))

$$\lim_{\delta t \to 0} E\left(f(t)f(t')\right) = c\delta(t - t')$$

where $\delta(t - t')$ is the distribution function called *Dirac's delta function.* Using this formalism we can say that Wn is a statistical process where a Gaussian-distributed random variable $f(t)$ with

$$E\left(f(t)\right) = 0 \text{ and } E\left(f(t)f(t')\right) = c\delta(t - t^{\prime)} \tag{2.7}$$

is assigned at each time t.

In order to investigate the relations between Wn and Bm, we analyze the random variable $f(t)$ in the frequency domain with the help of Fourier transform

$$\phi(\nu) = \int_{-\infty}^{+\infty} f(t)e^{-2\pi\nu t}\, dt \tag{2.8}$$

In other words, $\phi(\nu)$ can be seen as a linear combination of the values $f(t)$. As a consequence, both the real and imaginary parts of the Fourier

transform $\phi(\nu)$ are Gaussian-distributed random variables, too. From 2.8 and the definition of Wn 2.7 we obtain

$$E\phi\left((\nu)\right) = \int_{-\infty}^{+\infty} Ef(t)e^{-2\pi i\nu t}\,dt$$

Can be shown (Sornette (2000)) that also the second momentum of the distribution, $E\left(f(t)f(t')\right)$, can be expressed in terms of Dirac's delta function

$$E\left(\phi(\nu)\phi(\nu')\right) = c\delta(\nu - \nu')$$

Thus, Wn can be uniquely characterized by the properties of its Fourier amplitudes $\phi(\nu)$ instead of the original representation $f(t)$.

Because in the Bm the random variables are represented by the particle's displacements we can say that Bm arises from integrating Wn

$$E\left(\phi(\nu)\phi(\nu')^*\right) = \frac{c}{2\pi i\nu\left(2\pi i\nu'\right)^*}\delta(\nu - \nu') = \frac{c}{(2\pi\nu)^2}\delta(\nu - \nu')$$

so that we can think of Bm as a statistical process where $\phi(\nu)$ are Gaussian-distributed random variables with

$$\phi(\nu) = 0 \text{ and } E\left(\phi(\nu)\phi(\nu')^*\right) \sim \nu^{-2}\delta(\nu - \nu').$$

2.2.2 Fractional Brownian motion and its scaling properties

What we obtained for Wn and Bm can be expressed as follows

$$E\left(\phi(\nu)\phi(\nu')\right)^* = P(\nu)\delta(\nu - \nu')$$

where $P(\nu)$ is constant for Wn and decreases like ν^{-2} for Bm. The function $P(\nu)$ is denoted as *power spectrum* of the process.

A generalization to a power-law function $P(\nu)$ with arbitrary exponents, leads directly to the *Fractional Brownian motion* (fBm); it is a statistical process where both the real and imaginary parts of the Fourier amplitudes $\phi(\nu)$ are Gaussian-distributed random variables with

$$\begin{cases} E\left(\phi(\nu)\right) = 0 \text{ and } E\left(\phi(\nu)\phi(\nu')^*\right) = P(\nu)\delta(\nu - \nu') \\ P(\nu) \sim |\nu|^{-\beta}. \end{cases}.$$

Let us note that Wn is a fBm with $\beta = 0$, while Bm is a fBm with $\beta = 2$.

Defining a *fractional derivative* as

$$\frac{\partial^\alpha}{\partial t^\alpha} f(t) = \int_{-\infty}^{\infty} \phi(\nu)(2\pi i\nu)^\alpha e^{2\pi i\nu t}\,d\nu$$

for arbitrary real number α and applying it for negative values α, we get *fractional integration*. In this sense, fBm with a spectral exponent β arises

from applying the fractional integration with $|\alpha| = \frac{1}{2}\beta$ to Wn. In Fig. 2.3 examples of fBm for different spectral exponents β between 0 and 3 are given.

Let's recall that our target is to quantify the differences in roughness shown by the seismic noise records (see Fig. 2.1). Fig. 2.3 shows that the spectral exponent β is linked with both such differences and the scaling properties of the process $f(t)$ that represents our seismic noise records. As a consequence, we have to study the scaling properties of the fBm. For

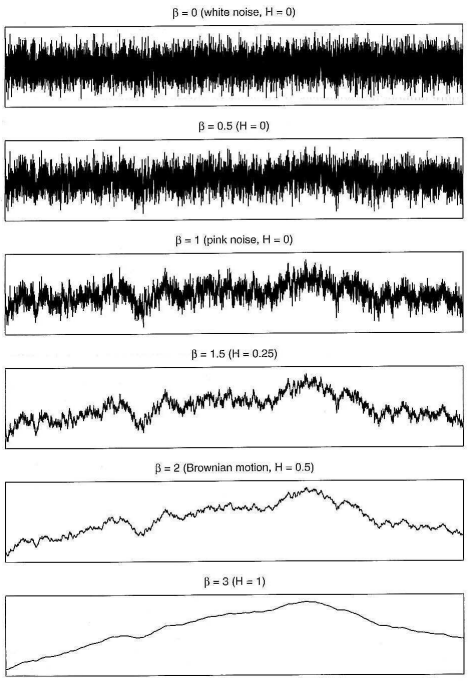

Figure 2.3: *Examples of fBm with different spectral exponents β between* 0 *and* 3. *The signal $f(t)$ is plotted versus t in arbitrary units. The quantity H represents the Hausdorff exponent. From Hergarten (2002)*

such purpose the starting point is to define e new process called *self-affine fractal;* we say that a random process $f(t)$ is a self-affine fractal if all random processes $f_{\lambda,\tau}(t)$ which arise from the transform

$$f_{\lambda,\tau}(t) = \lambda^H f\left(\frac{t-\tau}{\lambda}\right)$$

are characterized by the same statistical properties. The parameters λ and τ represent the spatial and temporal scaling factors, respectively. The exponent H is called *Hausdorff exponent.*

A fBm is a self-affine fractal because can be shown (Sornette (2000)) that its rescaled Fourier amplitudes $\phi_{\lambda,\tau}(\nu)$ are Gaussian-distributed random

variables with

$$E\left(\phi_{\lambda,\tau}(\nu)\right) = \lambda^{H+1} e^{-2\pi i\nu\tau} E\left(\phi(\lambda\nu)\right) = 0 = E\left(\phi(\nu)\right)$$

and

$$E\left(\phi_{\lambda,\tau}(\nu)\phi_{\lambda,\tau}(\nu')^*\right) = \lambda^{2H+1-\beta} E\left(\phi(\nu)\phi(\nu')\right).$$

We can conclude that the statistical properties of fBm persist under anisotropic scaling exactly if $2H + 1 = \beta$. As a consequence, fBm is a self-affine fractal with Hausdorff exponent

$$H = \frac{1}{2}(\beta - 1). \tag{2.9}$$

Can be shown (Sornette (2000)) that the admissible numerical values for the Hausdorff exponent in order to preserve the scaling properties of a fBm must be in the range

$$0 \leq H \leq 1 \text{ and } 1 \leq \beta \leq 3 \tag{2.10}$$

for the Hausdorff and spectral exponent, respectively. The H exponent is for a description of the process in time-domain while the β exponent is for a description in frequency domain, the link between them is expressed in 2.9 so that we can switch from one description to the other one, through 2.10, according to our needs.

2.2.3 Recognizing fBm

Temporal correlation can be quantified by the so called *variogram* $\Gamma(t,\tau)$ (Matheron (1963))

$$\Gamma(t,\tau) = E\left(f(t+\tau) - f(t)\right)^2 \tag{2.11}$$

which describes the spreading of the probability density through time. The variogram is the generalization of the time-dependent variance $\sigma(t)^2 = E\left(f(t)^2\right)$ towards functions which do not satisfy the condition $f(0) = 0$ assumed when we have introduced the Brownian motion. It can be shown (Sornet, 2002) that for $1 < \beta < 3$ the variogram $\Gamma(\tau)$ can be expressed as

$$\Gamma(\tau) \sim \tau^{\beta-1}. \tag{2.12}$$

where we have omitted the argument t because $\Gamma(t,\tau)$ depends on the time lag τ only.

We note that the definition of the variogram 2.11 involves expected values in the statistical sense; so, the variogram can not be computed directly from a given time series that is why we refer to 2.12 as *theoretical* variogram. Instead, the expected values must be estimated from the values $f(t)$. The

best estimate is obtained from averaging over the available range in time. If the time series is observed within an interval $[T_1, T_2]$, this leads to

$$\Gamma(\tau) \approx \frac{1}{T_2 - T_1 - \tau} \int_{T_1}^{T_2-\tau} (f(t+\tau) - f(t))^2 \, dt.$$

If the available data are restricted to discrete times $t_1, t_2, \cdots, t_n$, the integral must be approximated by a discrete sum. For a constant sampling rate $\delta t = t_{k+1} - t_k$ we can approximate the integral for constant time lags $\tau = k\delta t$ as

$$\Gamma(k\delta t) \approx \frac{1}{n-k} \sum_{i=1}^{n-k} \left(f(t_{i+k} - f(t_i)\right)^2. \tag{2.13}$$

So, after the variogram has been estimated by 2.13, the result must be compared with the theoretical result 2.12. If $\Gamma(\tau) \sim \tau^\alpha$ with $0 < \alpha < 2$, equation yields $\beta = 1 + \alpha$. The scaling exponent α has no physical meaning, Husdorff exponent H is linked with the scaling properties of the fBm. Recalling that $2H + 1 = \beta$, the link from what is estimated from data, i.e., the scaling exponent α, and H is $\alpha = 2H$.

2.2.4 Predictability

How the statistical properties of time series and their scale invariance are linked with the dynamical behavior of the scaling properties, is the topic called *predictability of the process*. We do this with respect to fBm.

Let us assume that the recent value $f(t)$ and perhaps an older value $f(t-\tau)$ are known, and we are aim at predicting $f(t+\tau)$. We construct the prediction linearly from the recent value $f(t)$ and the trend between previous and recent value, $f(t) - f(t-\tau)$

$$f_p(t+\tau) = \lambda f(t) + \mu \left(f(t) - f(t-\tau)\right)$$

where $f_p(t+\tau)$ is the predicted value and λ e μ are constants. Obviously, the quality of the prediction must be assessed statistically; the mean quadratic error $\sigma_p^2(\tau)$ defined by

$$\sigma_p^2(\tau) = E\left(f_p(t+\tau) - f(t+\tau)\right)^2$$

provides a straightforward measure. It can be shown that the best prediction for $f_p(t+\tau)$ is

$$\begin{cases} f_p(t+\tau) = f(t) + \left(2^{\beta-2} - 1\right)\left[f(t) - f(t-\tau)\right] \\ 1 < \beta < 3 \end{cases}. \tag{2.14}$$

This means that the actual value $f(t)$ is still a good basis for predicting $f(t+\tau)$. However, the trend from the past must be regarded in a different

way. If $\beta > 2$, the best prediction $f_p(t+\tau)$ is still larger than $f(t)$ if the signal increased in the past. This means that the trend of the signal tends to persist. In other words, the signal is likely to increase in the future if it has increased so far, and vice versa. This property is called *persistence.* If $\beta < 2$, the behavior is opposite. If the signal has increased, it is likely to decrease in the future, and viceversa. This property is called *anti-persistence.* If $\beta = 2$ from 2.14 emerges that the past plays no role in predicting $f(t)$, the increments are independent. In other words, the process is Bm and it is just at the edge between persistence and anti-persistence.

2.3 Conclusive remarks

We have already noticed that the measured parameter from data is the scaling exponent α, but it has no physical meaning. Who has such meaning is the Hausdorff exponent H if we work in time domain, or the spectral exponent β if we work in frequency domain. So in terms of scaling exponent, taking into account that $\alpha = \beta - 1$ and $2H + 1 = \beta$ so that $\alpha = 2H$, we can summarize the results concerning the predictability obtained in the previous paragraph as

$$\begin{cases} \text{Brownian motion} & \alpha = 1 \text{ diffusive process} \\ \text{persistence} & \alpha > 1 \text{ superdiffusive process} \\ \text{anti-persistence} & \alpha < 1 \text{ subdiffusive process} \end{cases}$$

Our target was to characterize the roughness of the displacement of the noise records (Fig. 2.1). On theoretical basis previously discussed, in the paper **P2** the average squared soil displacement $< r^2(\tau) >$ has been evaluated using the variogram method as function of the time scales τ. The results have been

- seismic noise is neither White noise nor Brownian stochastic process;
- it is a self-similar (or fractal) stochastic process that can be described in terms of persistent fBm ($H > 0.5$);
- a dependence of statistical features of the soil motion on the geological nature of the site has been shown to exists.

It is worth noticing that on the contrary of the deterministic approach, such results have been reached without need of any *a priori* hypothesis neither on the noise field nor on its spectrum.

Chapter 3

Soil shaking features: experimental approach

The evaluation of the characteristics of the strongest expected ground shaking for specific areas of the site under study is a basic tool for high-priority actions aimed at mitigating the seismic risk. This is particularly true in urban areas being these latter more safety demanding. Such target can be achieved through studies concerning the site effects, as we have seen before. In studying site effects the so called *experimental approach* can not be disregarded. This latter consists in directly measuring the response of the site under study through records of both regional as well as local earthquakes. The analysis of such records allows to investigate the soil shaking features with the aim of understanding the observed damage pattern, often unexpected, at the surface.

As already mentioned, we have chosen as case study the city of Rome also because its large concentration of monuments and ancient buildings, many of which have assumed political and strategical relevance. Because of their extreme vulnerability, the evaluation of the characteristics of the strongest expected ground shaking for specific areas of the city is a basic tool for any high-priority action aimed at mitigating potential damages that could arise from earthquakes.

The city of Rome during its long history suffered damage up to intensity VII-VIII of the Mercalli-Cancani-Sieberg scale due to the largest earthquakes in the Apennines (see Molin and Guidoboni (1989)). In the city, the occurrence of the strongest damage episodes seems to be restricted to the Holocene alluvial areas (Ambrosini et al. (1986); Salvi et al. (1991)), with a significant concentration close to the edges of the main sedimentary body of the city: the Tiber river valley (Fig. 3.1).

Unfortunately, no strong-motion recordings were available until 2008 for the city of Rome which makes it impossible any estimate based on actual measurements of ground motion induced by earthquakes. That is why it

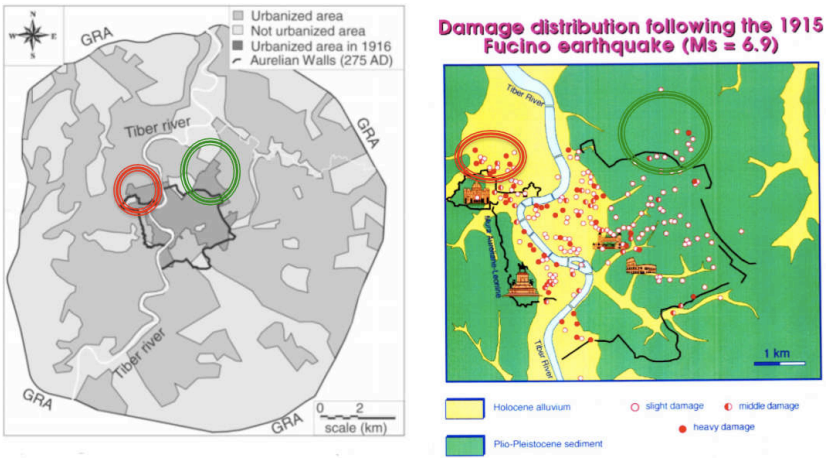

Figure 3.1: *Left panel: city of Rome, present urbanized area within the ring-road (GRA). The dark gray area represents the urban settings after the 1915 Fucino earthquake., from Cifelli et al. (2000). Right panel: sketch of the simplified near-surface geology showing the damage pattern experienced during the 1915 Fucino earthquake. The red and green circles are for comparing the damages (right panel) with the urbanized areas (left panel). From Ambrosini et al. (1986) and Cifelli et al. (2000).*

has been decided to realize a 5-station 3D seismic array of seismic stations (Fig. 3.2). This has been realized within two multidisciplinary research projects: FIRB 2002-2005 (code: RBAU01JMT3), and COFIN 2004-2005 (code: 2004041297-002). In the first one the author of the present thesis has been the scientific responsible for the Research Unit 3, whereas in the second one he has been scientific responsible for the I.N.G.V.

More in details, the projects involved the installation of a permanent seismic array and a detailed classification of the physical and mechanical properties of the rocks constituting the geological subsoil of Rome, under both static and dynamic conditions. 1D numerical models of local seismic response to possible strong motion (PGA of up to 0.06g) in the city of Rome were performed. These models highlight the important role that an up to 60m-thick silty-clay sedimentary pack inside the Tiber alluvia can play in terms of ground motion amplification (see **P3** and **P4**).

As a consequence of the aforementioned projects, since early 2008 a small-aperture four-station array has being operating on the alluvial sediments within the Tiber Valley in Valco San Paolo, in the southern part of the historical sector (Fig. 3.2). Interdistance between the array stations is up to 100 m. Another station was installed about 2 km east of the array, above the Pleistocene pyroclastic succession and the underlying, older sedimentary deposits of the Paleo-Tiber River (Marra and Rosa (1995)). These stations are composed of both strong-motion (accelerometers) and

weak-motion (LE-3D velocimeters by Lennartz) three-component transducers equipped with continuously recording 24-bit analog-to-digital converters at a sampling rate of 1000 Hz. Time synchronization is provided by a GPS system at each station. Moreover, one three-component short-period seismometer (Lennartz LE-3D/BH) was installed at the bottom of a 72 m deep borehole, within the Plio-Pleistocene clayey bedrock, 15 m below the base of the alluvial soft sediments. The borehole data are continuously recorded at the surface using the same acquisition system of stations deployed at the surface.

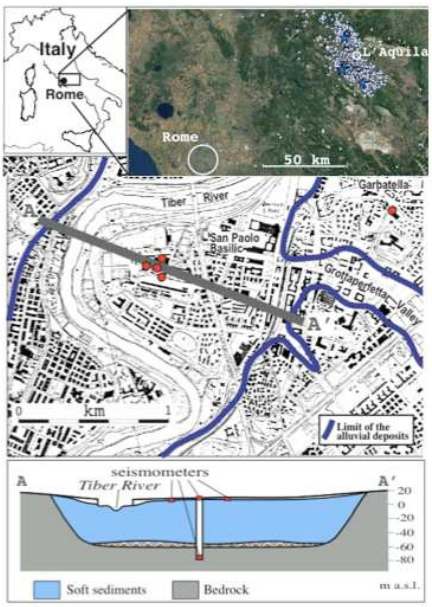

Figure 3.2: *Top panel: epicenter of l'Aquila 6th April 2009 Mw=6.1 damaging earthquake with the epicenters of the seismic sequence. Middle panel: 3D array location, red spots represent seismic stations. The red spot outside the Tiber valley (Garbatella) is the reference station. Bottom panel: sketch of the borehole station located beneath the alluvial sediments layer. See paper* **P2** *for details.*

On the 6th April 2009 a damaging earthquake hit the town of L'Aquila, central Italy. Thanks to the aforementioned array, it was recorded with its moderate-magnitude sequence of aftershocks, at 100 Km far in the city of Rome with a satisfactory signal-to-noise ratio for all events with $Mw \geq 4$ (Fig. 3.2). A moment magnitude of Mw 6.3 was promptly assessed by international agencies, however we adopt the value Mw 6.1 that better fits ground motion amplitudes of Italian broad-band stations at periods of 1 to 20 s when a local velocity model is used (Scognamiglio et al. (2010); Calderoni et al. (2009); Herrmann et al. (2011)). The earthquake struck a sector of the Central Apennines that is considered as the most potentially

dangerous seismogenic zone with earthquakes that can cause heavy damages in the city (Salvi et al. (1991)). Magnitudes as high as 7 are expected in that region. The most recent of these major earthquakes took place in 1915 near Avezzano, 80 km northeast of Rome (Fig. 3.1).

A study by Ambrosini et al. (1986) reported that the most severe damage caused by the 1915 Avezzano earthquake within the city of Rome was suffered by buildings located on the Holocene alluvial fill of the Tiber valley (Fig. 3.1), thereby stressing the role of local geology in amplifying ground shaking. Accordingly, monuments erected on soft layers were affected by site effects in their long life (Boschi et al. (1995); Moczo et al. (1995)). Studies aimed at quantifying the effects of local geology, including 2D modelling using finite-difference techniques as well as hybrid techniques, deterministic and stochastic ones, were conducted since the early '90 (Fäh et al. (1993); Rovelli et al. (1994, 1995); Caserta et al. (1999)). 3D models, limitedly to a maximum frequency of 1 Hz, were performed for the city of Rome by Olsen et al. (2006). Numerical simulations of the soil shaking features in the city of Rome will be the topic of the next chapter, where will be discussed in details also the comparison between the synthetics seismograms and the real records of the l'Aquila sequence obtained by the previously described roman array.

Data recorded during the April 2009 seismic sequence are the first instrumental data ever recorded in the city of Rome by an array of seismic stations, that is why they yield an unprecedented information to assess ground motion local variations allowing us to check previous theoretical and numerical estimates of the seismic response of Rome adding new quantitative information on regional and local effects with important implications for a better constrained hazard assessment of the city.

3.1 Geological settings of the city of Rome

Although the early settlements of ancient Rome were established on the famous "Seven Hills", the city soon expanded over the large alluvial plain of the Tiber River and its tributaries. Nowadays, more than one half of the "Historical Center" is built over these soft fluvial deposits (Fig. 3.1). Similarly, a large part of the most recently built portion of the city is located above the thick alluvial filling of the Holocene hydrographic network (see Fig. 3.3). This network originated during the Würm glacial (lasted until 18 ky) through re-incision and deepening of the valleys which had developed during previous glacial-interglacial phases (Marra et al., 2008). The role of these lateral variations on effects felt in Rome by the population during earthquakes is discussed in Cifelli et al. (2000).

The sediments filling the incision of the Tiber River within the city of Rome consist of a fining-upward succession, with a 6-8 m thick level of gravel

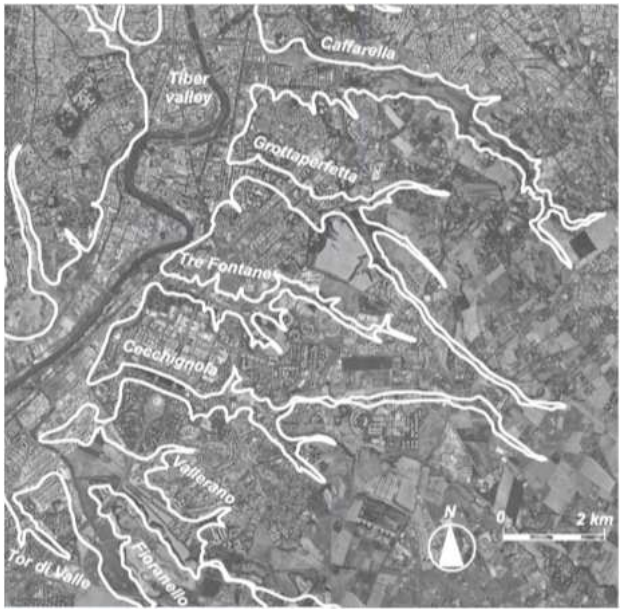

Figure 3.3: *Satellite image of the souther portion of the Rome's urban area showing the boundaries (white lines) of the left-side lateral alluvial valleys due to some of the tributaries of the Tiber River forming the Holocene hydrographic network.*

at the base and an overlaying 50-60 m thick pack of sand and clay (see **P3** and **P4**). This fine-grained portion of the deposit is represented by normally to weakly overconsolidated clay-sandy silt, saturated in water, with low deformability moduli (**P3**, **P4**). Within the central axis of the Tiber valley, the bedrock of the alluvial sediments is represented by a Plio-Pleistocene succession (Marra and Rosa (1995)), consisting of alternating, decimeter-thick levels of clay and sand, with an overconsolidation ratio (OCR) of > 5 and low compressibility (**P3**, **P4**). The upper portion of the valley sides, as well as the terrains out of the alluvial plains, where the rest of the city is built, are composed of Pleistocene fluvial deposits (the Paleo-Tiber unit, see Marra and Rosa (1995); Florindo et al. (2007)), comprising a 10 m thick layer of coarse gravel followed by consolidated sandy clay, and by a thick volcanic cover, represented by more or less lithified pyroclastic-flow deposits and alternating ash-fall deposits (Karner et al. (2001)), partially intercalated into the continental sedimentary deposits Karner and Marra (1998)).

3.2 Data analysis

In this paragraph two things are discussed based on the 2009 dataset:

- spatial variations of ground motion in Rome between closely located

sites on Holocene vs Pleistocene sediments;

- comparisons with ground-motion predictions equations (GMPEs) based on larger Italian and global datasets.

To do that we have analyzed the records of the mainshock and the strongest aftershocks (events are listed in Tab. 3.1) at three stations, in different geological units: outcrops of sedimentary Holocene alluvium (station VSC), outcrop of volcanic Pleistocene deposits (station GRB) and in the bedrock Pliocen clay by using the borehole station (BRH). Among the array stations, we selected the one affected by the lowest cultural noise. We have used the accelerometric records of the two surface stations, VSC and GRB, and the velocity record of the borehole station, BRH. Accelerograms were processed

Date	Time (UTC)	Lat (deg.)	Lon (deg.)	Depth (Km)	Mw
2009/04/06	01:32:39	42.334	13.35	8.8	6.1
2009/04/06	02:27:46	42.375	13.342	10.0	4.1
2009/04/06	02:37:04	42.366	13.340	10.1	4.8
2009/04/06	04:47:53	42.352	13.347	9.4	3.8
2009/04/06	07:17:10	42.355	13.367	9.2	4.0
2009/04/06	16:38:09	42.362	13.333	10.2	4.3
2009/04/06	21:56:53	42.396	13.323	9.7	3.8
2009/04/06	23:15:37	42.451	13.364	8.6	4.8
2009/04/07	09:26:28	42.342	13.388	10.2	4.8
2009/04/07	17:47:37	42.275	13.464	15.1	5.4
2009/04/07	21:34:29	42.380	13.376	7.4	4.2
2009/04/07	21:39:06	42.361	13.363	10.4	3.6
2009/04/09	04:32:44	42.455	13.420	8.1	4.1
2009/04/09	04:43:09	42.506	13.366	9.2	3.7
2009/04/09	19:38:16	42.501	13.356	17.2	5.0
2009/04/10	03:22:22	42.470	13.417	9.4	3.7

Table 3.1: *Date and source parameters of earthquakes analyzed in this study. Hypocenter determinations are from the INGV bulletin (at http://iside.rm.ingv.it.), and moment magnitudes Mw from Herrmann et al. (2011).*

according to the Boore (2005) and Boore and Bommer (2005) approach, a 4-pole acausal 0.1 Hz high-pass Butterworth filter was applied; the integration of corrected accelerations in the time domain yielded velocity and displacement time series.

3.2.1 Ground motion features

During the main shock, ground motions were as large 15 cm/s^2, 3.1 cm/s and 1.3 cm in terms of acceleration, velocity, and displacement, respectively (Fig. 3.4). This figure indicates that GRB and VSC show a small difference in the displacement waveforms, apart from small-amplitude but persistent resonating reverberations that are evident in the Tiber valley between 20 and 50 s. In contrast, the difference is significant in the velocity and acceleration

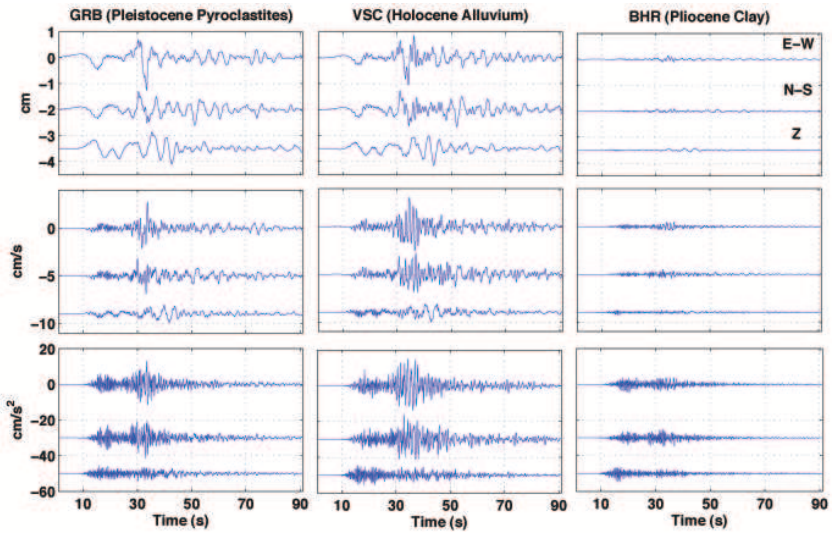

Figure 3.4: *Displacement, velocity and acceleration time series (EW, NS and vertical component corresponds to the top, middle, and bottom trace, respectively) recorded in Rome on different geological units during the main shock of the April 2009 seismic sequence.*

time series, the nearly harmonic excitation of the alluvial deposits dominating in amplitude the velocity and acceleration time series. The borehole records show a strong depletion of amplitudes, mostly for the displacement and velocity time series. This is partly due to both the sediment and free surface effects.

More in detail, in Fig. 3.5, left panel, a comparison is shown of the displacement (radial, R, and transversal, T, component) on GBR and on VSC. Note similarity of waveforms shapes and amplitudes, with VSC being somewhat larger than GRB on the T component. Note also that the dominant period is near 5 s, so these graphs indicate that there is little relative site response at long periods (periods near 5 s). On the contrary, in looking at the right panel, where the comparison is made using velocities, we note that there is less agreement in waveforms shapes and amplitudes than for the displacement time series, and VSC is much larger than GRB on the T component. These graphs suggest that there is relative site response at shorter periods, at least for the T component.

Ground motions recorded in Rome during the April 2009 seismic sequence are also valuable because they illustrate the role of the different seismic phases radiated toward Rome by earthquakes of engineering interest occurring in the central Apennines. To this purpose, the parameter

$$I_a(t) = \frac{2\pi}{g} \int a^2(t')dt' \tag{3.1}$$

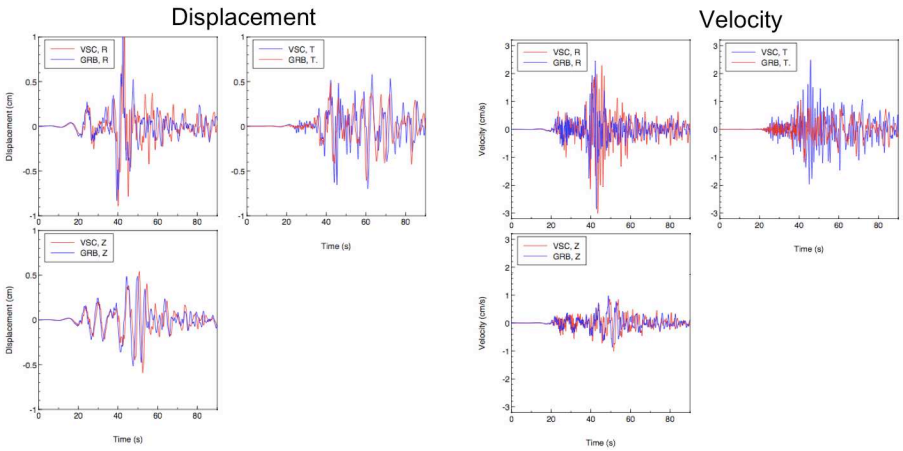

Figure 3.5: *Left panel: comparison of displacement traces at VSC and GRB. The displacements were obtained by double integration of acceleration band pass filtered between 0.1 and 10 Hz. Right panel: comparison of velocity traces at VSC and GRB.*

is plotted in Fig. 3.6 top panel. When the integral is computed over the duration T necessary to reach the asymptotic plateau, equation 3.1 yields the Arias intensity $I_a(t)$ (Dobry et al., 1978). Fig. 3.6 (top panel) shows that there is a sharp increase of the energy rate around t=30 s. This is a common feature to the three stations, but the alluvial deposit resonance at VSC amplifies $I_a(t)$ by a factor of 2 above the one of volcanic rocks of GRB. The $I_a(t)$ curve of the borehole station is a factor of 10 smaller. From Fig. 3.6 (bottom panel) it emerges that the main role on the energy rate is played by the wave starting around t=30 s, which increases sharply the cumulative curve in a time window of about 10 s (from t=30 to 40 s, approximately).

In order to better quantify the site response we use spectra and their ratios. Let start computing the Fourier amplitude spectra (FAS) of single components for all three stations. FAS in Fig. 3.7 give a more direct indication of station-to-station site response than the previous figures. It does show clearly that there is little or no relative site response for frequencies less than about 0.4 Hz or greater than about 5 Hz. The figure also shows clearly that BRH motions are considerably smaller than the VSC motions. The largest difference between VSC and GRB seems to be on the T component, but it might be misleading to focus on ratios of individual components if lateral refraction has occurred. This leads in computing the ratios of geometric means of the two horizonal components, averaged over many events. In Fig. 3.8 are shown the observed VSC/GRB and VSC/BRH spectral ratios of FAS for the R and T component of both the main shock and the average spectral ratios over a subset of events made by 9 aftershocks, extracted from those listed in Tabel 1, with a signal-to-noise ratio higher than

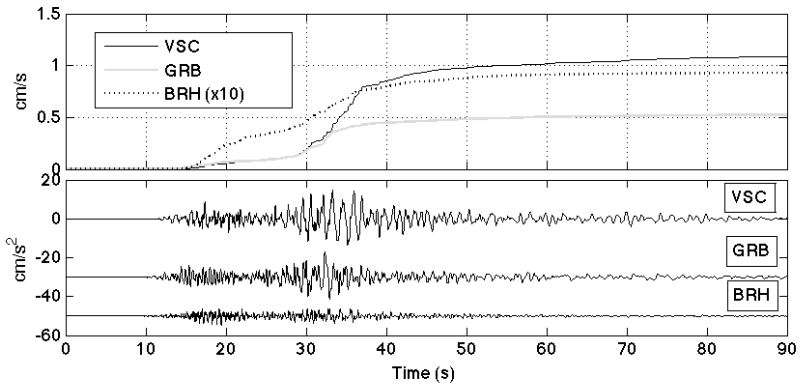

Figure 3.6: *Top panel: cumulated squared accelerations (Equation 1) of the borehole BRH and the two surface stations VSC and GRB. The BRH result is multiplied by a factor of 10 for a better visual inspection. Bottom panel: recorded accelerations (EW component) of the three stations.*

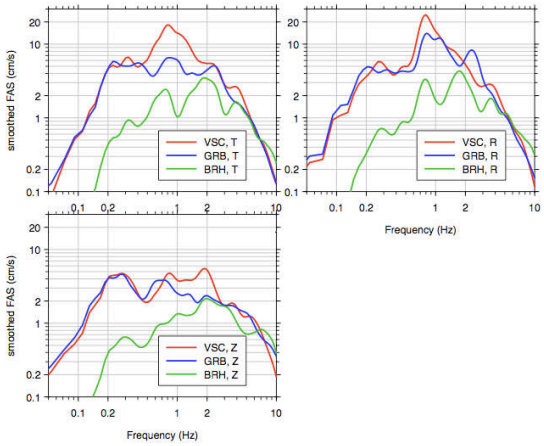

Figure 3.7: *Fourier amplitude spectra (FAS) for VSC, GRB and BRH. Single component, three stations per panel.*

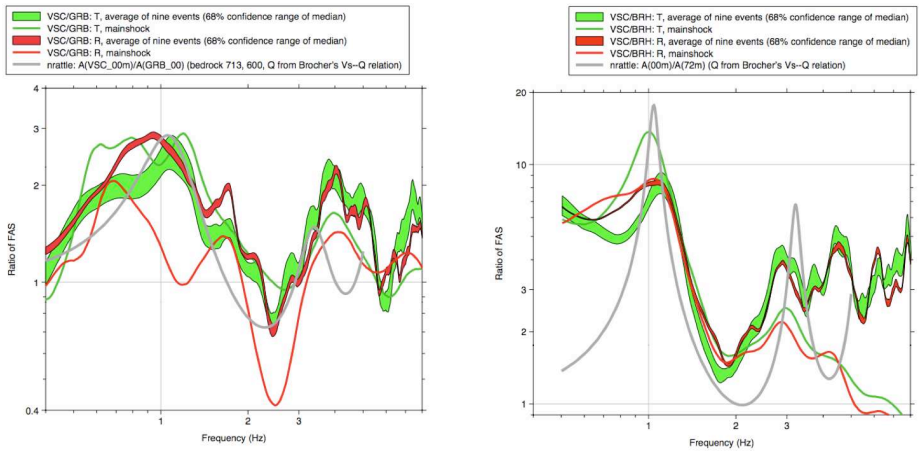

Figure 3.8: *Left panel: observed and simulated VSC/GRB ratios of FAS. Right panel: observed and simulated VSC/BRH ratios of FAS. In both panels are shown ratios for the mainshock (for R and T component), 68% confidence interval of the median of the ratio of nine events and the theoretical ratio for the 1D model and the plane-wave excitation (Boore, private comunication).*

3 in the frequency band 0.5-10 Hz. In looking at Fig. 3.8 left panel, we see a satisfactory agreement between the mainshock and the aftershocks for both R and T components around 1 Hz, i.e., the main peak in the spectral ratios. Such agreement is more satisfactory considering the error concerning the aftershocks are very narrow for R as well as T components.

Fig. 3.8 compares also such spectral ratios with the theoretical ratio calculated in a conventional 1D approach (plane-wave and viscoelastic approximation) using the Vs vertical velocity profile derived from down-hole in situ measurements of paper **P3** slightly modified as in Tab. 3.2

lithology	**thickness m**	**Vp m/s**	**Vs m/s**	**density g/cm^2**	**Qp**	**Qs**
silty-sands	1.5	560	220	1.8	20	20
silty-sands	7.5	1480	239	1.84	20	20
silty-sands	12	1480	260	1.83	30	30
clayey-silts	13	500	190	1.83	20	20
clayey-silts	16	1280	235	1.83	30	30
sands	5.5	1600	417	1.92	30	30
bedrock	∞	2200	713	2.1	50	50

Table 3.2: *1D vertical velocity profile modified from* **P3** *extending the gravel layer (713 m/s) to the whole bedrock.*

The spectral ratio VSC/GRB results in a satisfactory agreement with the theoretical spectral ratio, and both confirm the validity of the previous theoretical 1D predictions of this resonance (e.g. Boschi et al. (1995) and the papers **P3** and **P4**, to quote only one of the first and one of the last papers dealing with that issue).

The peak at 4 Hz is fitted neither by VSC/GRB nor by VSC/BHR spectral theoretical 1D ratios. Moreover, VSC/BHR spectral ratio for the mainshock considerably decreases after 2 Hz from those concerning the aftershocks. Up to now we have to say that we have no explanation for such behavior.

3.2.2 Ground-motion prediction equations analysis

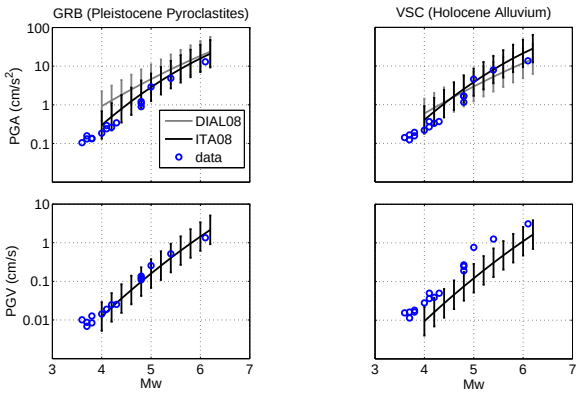

Figure 3.9: *Peak ground motions recorded in Rome during the April 2009 seismic sequence. Bars represent the ±1 standard deviation uncertainty of predictive equations by Bindi et al. (2009) and Alessandro et al. (2008) (indicated as ITA08 and DIAL08, respectively). Both these regressions are based on Italian data only. ITA08 curves are relative to class B and C for a comparison volcanic rock, and alluvium data, respectively. DIAL08 applies Class I and IV, respectively, of their own predominant-period site classification.*

The ground motion scaling versus magnitude observed in Rome during l'Aquila earthquake, is presented in Fig. 3.9, compared with expectations based on recent predictive equations using the Italian data bank (namely Alessandro et al. (2008) and Bindi et al. (2009)). We can note that observed accelerations are fairly well matched by predictions for all the geological units. The same happens for the observed velocities at stiff sites whereas they are at the border of 1 standard deviation. Also response spectra of VSC exceed those of GRB. Fig. 3.10 shows elastic absolute acceleration response spectra for 5% damping during the main shock, computed for the

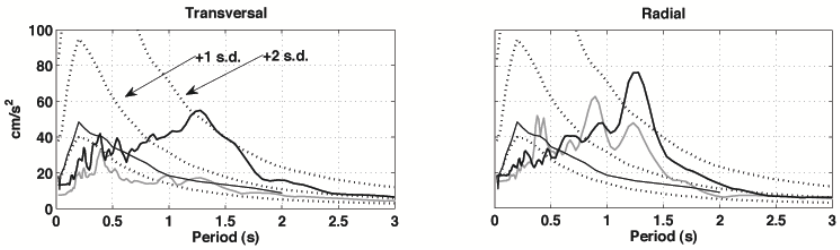

Figure 3.10: *Response spectra of the horizontal (radial and transversal) components: full black and gray curves are VSC and GRB, respectively. The thin black curve corresponds to the predictive equations by Bindi et al. (2009), in particular for the epicentral distance of 100 Km. The three dotted curves are predictions by Cauzzi and Faccioli (2008) for soft sites (average, average + 1 standard deviation, and average + 2 standard deviations).*

radial and transversal components for VSC and GRB stations. For both stations, spectral ordinates of the radial component are larger than those of transversal one. In Fig. 3.10 the response spectra are compared with regression curves for Class C of CEN (2004), for the epicentral distance of 100 Km, based both on worldwide data (Japan, USA, Iran, Turkey, Europe, see Cauzzi and Faccioli (2008), and Italian data only (Bindi et al. (2009)). Note that the contribution to spectral ordinates, in the range less then 0.5 s, is significantly below the expectation whereas at periods between 1 and 1.5 s observations exceed predictions by more than 2 standard deviations. More in details, see that the observed spectral ordinates exceed predictions up to more than 2 standard deviations for both radial and transversal components at VSC, and for the radial component at GRB. An excess by more than 2 standard deviations is systematic in the response spectra, being definitely confirmed by aftershocks shown in Fig. 3.11.

The conclusion is that, at long periods, not only soft sites but even stiff sites in Rome can suffer earthquake induced motions larger than expected on the base of the existing predictive equations. It has to be recalled that the joint contribution of regional propagation and local amplification at periods around 3 s caused a selective damage with destructive effects to several tall buildings in the lake-bed zone of Mexico City during the 1985 Michoacan earthquake, located more than 300 km away from the city (Singh et al. (1988); Singh and Ordaz (1993)). In that occasion, even the hill zone experienced large amplitudes at long periods. So, such effect is not unknown but this is the first time that it is observed and quantified for the city of Rome.

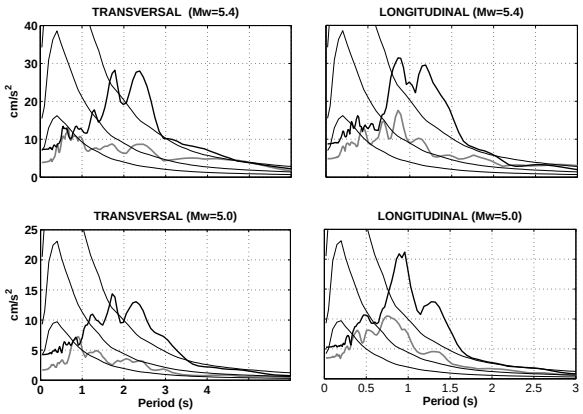

Figure 3.11: *Observed response spectra of the two strongest aftershocks (April 7 at 17:47 and April 9 at 19:38, in the upper and lower panels, respectively). Spectral ordinates at Holocene alluvium and Pleistocene pyroclastic sites correspond to the full black and gray curves, respectively. The three thin curves are the Class C predictions by Cauzzi and Faccioli (2008) (average, average + 1 standard deviation, and average + 2 standard deviations). Aftershocks confirm that observations exceed predictions by more than 2 standard deviations at periods between 1 and 1.3 s.*

3.3 Conclusive remarks

Instrumental data recorded in Rome during the April 2009 seismic sequence in central Italy indicate that the contribution to response spectra at short ($T < 0.5s$) periods is smaller than expectations (Fig. 3.10) . In contrast, longer period excitation is strong, especially between 0.5 and 2 s of the radial component. The causative earthquakes of the April 2009 seismic sequence were characterized by shallow ($\sim$ 10 km) depths and normal-fault mechanisms (Herrmann et al. (2011)). Both the shallow depth and effects due to the crustal structure could be the cause of such strong amplification of long periods. Unfortunately these two distinctive features are also expected for the strongest potential earthquakes in central Italy, and an amplification between 1 and 1.5 s could affect a large part of Rome. The effect could be particularly dangerous for modern zones grown in sedimentary areas where tall (around 10-storey) buildings predominate.

In the hazard practice, the expected spectral ordinates are conservatively incremented by + 1 standard deviation to assess hazard parameters. This increment is evidently too small: the April 2009 data show that even 2 standard deviations could be not conservative enough for Rome. A specifically determined increment is mandatory for the hazard assessment of the city.

Chapter 4

Soil shaking features: numerical simulation approach

Understanding, modeling and predicting ground motions produced by earthquakes belong to the high-priority problems of the seismic hazard assessment. That is why the development of techniques able to infer the spatial variability of ground motion during earthquakes is particularly important. Such spatial variability is caused by the interaction between seismic wave propagation and near-surface geology; an important contribution in this topic arises from studies involving the site effects as we have seen in Chapter one and three.

Site effects can be studied using the data recorded during an earthquake, an example is given in the previous Chapter, but because it would be useful to know the site characteristics of ground motion before an earthquake occurs, numerical modelling seems to be a useful method. This is particularly true in urban areas for planning actions aimed, among others, at mitigating the seismic risk. For such purposes we have chosen as site test, as already explained in the previous Chapters, the city of Rome.

The city during its long history suffered damage up to intensity VII-VIII of the Mercalli-Cancani-Sieberg (MCS) scale (Sieberg (1930)) due to the largest earthquakes in the Apennines (see Molin and Guidoboni (1989)). In the city, the occurrence of the strongest damage episodes seems to be restricted to the Holocene alluvial areas (Ambrosini et al. (1986); Salvi et al. (1991)), with a significant concentration close to the edges of the Tiber river valley (Tertulliani and Riguzzi (1995)). Molin and Guidoboni (1989) first performed an accurate revision of the historical sources concerning the earthquakes felt in Rome. Tab. 4.1 lists the most important earthquakes that were felt in the city of Rome during its long history. This summary shows that the destructive earthquakes that may affect Rome occur mainly

Data	I_0	I_R	Origin Area
83 B.C.	—	—	Unknown
72–70 B.C.	—	—	Unknown
51	—	—	Unknown
443	—	—	Unknown
484 or 508	—	—	Unknown
801	—	VII–VIII	Central Apennines
1349	X	VII–VIII	L'Aquila
1703	X	VII	L'Aquila
1812	VII	VII	Rome
1899	VII–VIII	VI	Albani Hills
1915	XI	VI–VII	Fucino

Table 4.1: *Strongest local and regional earthquakes felt in Rome (Molin and Guidoboni (1989)). I_0 is the epicentral MSC intensity; I_R is the intensity estimated in Rome.*

within two distinct seismogenic districts: the Alban Hills region, located approximately 25 km from the center of Rome, and the Central Apennines, located in a distance range 80-170 km from Rome. Figure 1 shows the epicentral location of earthquakes reported by the catalogue.

The Alban Hills have been investigated in detail, concerning both the characteristics of the local seismicity (Amato et al. (1994); Chiarabba et al. (1994)) and its recurrence and magnitude pattern (Basili et al. (1995)). The hypocentral depth is typically in the range 3 to 6 km. In a study on the sequence of the events based on the statistics of the extreme values, Basili et al. (1995) found that the maximum expected magnitude for an earthquake occurring in the Alban Hills is 5.2.

On the contrary, the seismogenic structures of the Apennines are characterized by fault length usually in the range of 10-20 Km and exhibit prevalent normal faulting focal mechanisms (see for example Valensise and Pantosti (2001)) The hypocentral depth is generally in the range of 10-15 km. Paleoseismic studies show that the magnitude of these earthquakes might have been 7 or larger (Pantosti et al. (1996)). From such seismogenic district have been originated the strongest MCS intensities in the city (VII-VIII MCS for the 1349, 1703, and 1915 earthquake sequences; see Table 1). In respect of the city of Rome, earthquakes originated from Albani Hills are considered as local seismicity whereas those from Central Apennines represent the regional seismicity.

Unfortunately, no strong-motion recordings were available for the city of Rome, neither local nor regional ones. This made impossible estimates based on actual measurements of ground motion induced by earthquakes. In absence of instrumental data, the development of techniques able to infer

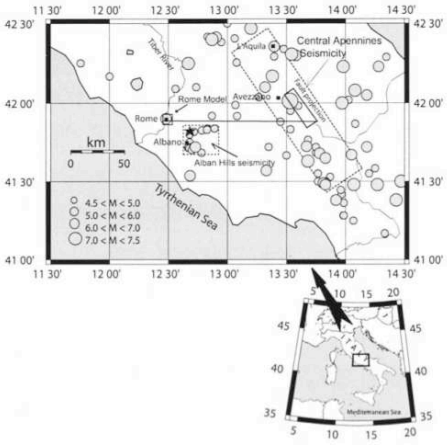

Figure 4.1: *The seismicity near Rome estimated from earthquakes of the Italian catalog, Catalogo Parametrico dei Terremoti Italiani (Gruppo di Lavoro, CPTI, 1999). Dotted rectangles present the two main seismogenic districts affecting the city (the Central Apennines and the Alban Hills). From Olsen et al. (2006).*

variability of ground motion during earthquakes is particularly important for a city like Rome as it is rich in ancient monuments and historical buildings, which are likely to be less resistant to the seismic action even in case of a moderate level of excitation. Numerical simulations of the soil shaking is one of the best approach for such purposes thanks also to the appearance of more powerful computers, better constrained basin models, and more efficient numerical wave propagation codes facilitated computation of 2D as well as 3D long-period seismic response of numerous sedimentary basins throughout the world (e.g., Frankel and Vidale (1992); Yomogida and Etgen (1993); Olsen and Schuster (1995); Olsen et al. (1995); Olsen and Archuleta (1996); Graves (1996); Wald and Graves (1998); Olsen (2000); Olsen et al. (2003)).

Numerical simulations concerning the sedimentary basin of Rome been perform since early 90's (Fäh et al. (1993); Rovelli et al. (1994, 1995); Moczo et al. (1995)). In full awareness that the computation of potential strong ground motions in different zones of the city is a fundamental tool to mitigate seismic risk and organize the public and private intervention priorities, Rovelli et al. (1994, 1995) proposed a hybrid technique simulation of the source and crustal path effects, able to generate a suite of synthetic accelerograms (SH waves) along 2-D profiles, whose amplitudes were modelled as a function of moment-magnitude, distance from the source, and local geology. Such hybrid technique is based on a use of stochastic procedures, proposed by Boore (1983), to generate a set of synthetic seismograms with the purpose of characterizing the seismic input to the rigid basement (bedrock) of

the city.

A similar hybrid method but based on a deterministic procedure, has been applied to the city of Rome by Fäh et al. (1993), who used the mode summation technique with a 2-D (P-SV) scheme of layered lithosphere to simulate the incoming wave-field to the bedrock of Rome generated by a ML = 6.8 earthquake, roughly 85 km east of the city.

Another hybrid technique has been proposed by Caserta et al. (1999) in order to combine deterministic and stochastic features. The aim is to describe the crustal propagation better than deterministic or stochastic methods can do separately. Indeed, in order to take into account effects due to small-scale heterogeneities of the crust, the authors added a stochastic noise (perturbation) to the signal propagated through the crust and numerically simulated in a deterministic way (P-SV waves) along a 2-D vertical section of the Tiber valley. The stochastic noise has been constructed using a kind of Markov-like process generator with two physical constraints: to have the Brune spectrum of the earthquake under study, and to reproduce the spatial decay of coherence, as reported in literature for real sites, directly in time domain. A Markow-like process generator allows to work directly in time domain, that is why the authors have chosen such stochastic approach.

One of the most recent simulations aimed at quantifying the effects of local geology on the soil shaking features for the city of Rome has been made by Olsen et al. (2006). They have generated a 3-D velocity model for Rome, embedded in a 1D regional model, and estimated long-period (1 Hz) ground motions from finite-difference simulations of viscoelastic wave propagation for two typical scenarios: an Albani Hills and a Central Apennines one. Their results showed that the strongest ground-motion amplification in Rome occurs in the Holocene alluvial areas, with strong basin edge effects in the Tiber River valley. What found by Olsen et al. (2006) was in agreement with earlier 2D SH-wave (Rovelli et al. (1994, 1995)) results showing amplification of peak velocities by up to a factor of 2 in the alluvial sediments, largest near the contact to the surrounding Plio-Pleistocene formations as also observed from the damage pattern by Ambrosini et al. (1986) for the Fucino 1915 earthquake.

All the aforementioned numerical simulations are lacking of knowledge concerning both the detailed near-surface geology and its geotechnical properties. Moreover, neither regional nor local events were recorded by seismic stations within Rome. Thanks to the already mentioned two multidisciplinary research projects (FIRB 2002-2005 and COFIN 2004-2005), data recorded in the city (l'Aquila 6th April 2009 sequence) are now available as well as detailed near-surface geology coupled with its geotechnical properties (see **P3** and **P4**). Such knowledge allows us not only to make more realistic numerical simulations using both detailed surface geology and actual elastic and inelastic parameters, but also to tune simulations of the soil shaking in order to better assess strong ground motion features through the whole city

as well as estimating parameters of engineering interest such as peak ground acceleration and velocity, Arias Intensity, response spectra, just to mention few.

4.1 3-D ground motion simulation

First our aim is to numerically reproduce the main features of the the spectral ratio content of soft/stiff, soft/bedrock and stiff/bedrock soils, i.e., VSC/GRB, VSC/BHR and GRB/BHR, respectively. For such purpose we need a subsurface model of Valco S. Paolo zone (Fig. 4.2), where the array is located.

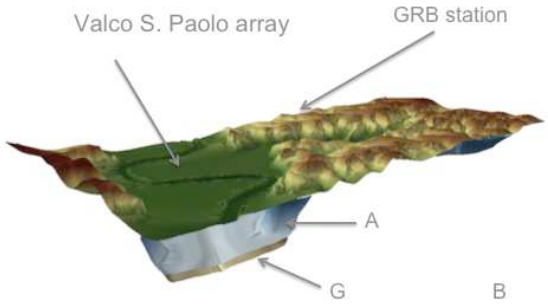

Figure 4.2: *Near-surface geological structure of Valco S. Paolo site used in numerical simulations. G is gravel layer, A is alluvium layer, B is bedrock (semi-space). Topography is from satellite Digital Elevation Model (DEM). Position of seismic array where both BHR and VSC stations are located, is shown. GRB reference seismic station position is shown as well.*

In Fig. 4.2 is sketched the 3-D near-surface geology of the Valco S. Paolo site used in the numerical simulations. The numerical values of the elastic and inelastic parameters are listed in Tab. 4.2. The velocity of the Alluvium layer has been obtained averaging the velocities of the layers inside the Tiber basin as they arose from **P3** and **P4** (see also Tab. 2 of the previous Chapter). Moreover, the parameters concerning the Gravel layer have been adopted for the whole semi-space, according to the 1D velocity model of Tab. 2 of the previous chapter.

For the purposes of our study, we adopted the serial code of Opršal et al. (2005); it is based on finite-difference technique on a Cartesian mesh (Opršal and Zahradnìk (2002); Opršal et al. (2005, 2004)), it computes the

	ρ g/cm^3	V_p m/s	V_s m/s	Q_p	Q_s
Recent Alluvium	1.83	1300	250	20	20
Gravel	2.10	2000	713	100	100

Table 4.2: *Elastic and inelastic parameters used in the numerical simulation. Gravel layer and semi-space (bedrock) have been assigned same numerical values*

full 3D seismic wave-field. Null normal stress boundary condition on the topographic surface is realized by the so-called vacuum formalism.

The adopted code is hybrid, effects of the source and the crustal propagation are numerically computed using discrete wave-number method (DW in the following; Bouchon (1981)), while the effects due to the near-surface geology, i.e., the site under study, is computed by a finite differences technique (FD in the following). To be more specific (Fig. 4.3), the complete wave field, i.e., that which is due to a given double-couple source, 1D crustal model and 3D site conditions, is a sum of the background and residual fields. The background field is due to the source in the 1D crust only; no 3D site propagation is included. The background and residual fields are coupled at the so-called outer and inner excitation lines, forming a double rectangular box attached to the free surface, and entirely enclosing the 3D site. The region between the inner excitation lines (inclusive) and the free surface is the excitation box (Fig. 4.3). All differences between the 1D and 3D models occur solely inside the excitation box. Inside the excitation box the complete wave field is numerically computed, while outside the excitation box (including the outer excitation lines) only the residual field is computed. Further interactions of the residual field with the crustal interfaces, which are all below the excitation box, are not considered. The background wave field, hereafter simply called the excitation, is calculated by the DW method, while all the numerical calculations inside and outside the excitation box (the complete and residual fields, respectively) are by FD method. Exact mathematical formulation, supplementing the above algorithmic description, can be found in Opršal et al. (2009).

The DW computation refers to source and crustal propagation so, we need: the location, hypocentral depth, focal mechanism and crustal model; we refer to the paper of Herrmann et al. (2011) for all such information. For the L'Aquila earthquake the focal parameters used in the DW simulation are: strike = 135^o, dip = 55^o and rake = -95^o. A point source at Lat = 42.339^o N, Lon = 13.371^o E and depth of 5 Km is used. The crustal model as it arises from Herrmann et al. (2011) holds for Central Apennines crustal region, in order to link it with the shallow layers of the roman area we have slightly modified their crustal model in the upper layers. In Tab. 4.3 the

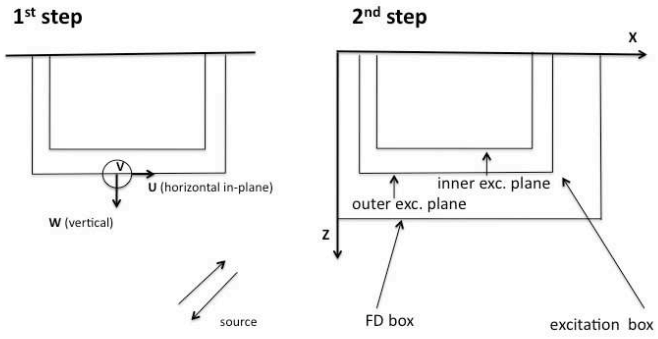

Figure 4.3: *Schematic representation of the DW-FD hybrid method. In the 1st step the source and the crustal path effects are calculated by the DW method, and stored at the excitation planes. A 2D vertical section of the 3D excitation box is shown. In the 2nd step the source is no more (instead of it there is the excitation box), but a 3D heterogeneity in included. The complete and residual fields are calculated by the FD method inside and outside the excitation box, respectively. The left, right and bottom sides of the FD box are nonreflecting, the top side is the free surface (topography).*

layer depth Km	V_p Km/s	V_s Km/s	ρ g/cm^3	Q_p	Q_s
0.0	2.00	0.713	2.0	100	100
0.3	2.00	0.800	2.1	150	150
0.7	3.00	1.500	2.2	250	250
1.2	4.00	2.000	2.2	350	350
1.7	4.80	2.500	2.2	400	400
2.7	4.90	2.600	2.3	450	450
3.7	4.90	2.700	2.3	500	500
7.7	5.60	3.100	2.4	500	500
15.7	6.10	3.400	2.4	500	500
25.7	6.30	3.500	2.5	500	500
31.7	7.80	4.300	2.5	500	500

Table 4.3: *Crustal model from Herrmann et al. (2011) slightly modified in the upper layers for linking with the shallow layers of the roman area.*

actual crustal model adopted in the DW simulations is shown. The Q values used in the model came from Brocher (2008) relation between Q and Vs.

Even thought we use a hybrid technique saving a big amount of computational time and memory, it is not enough to simulate big size domains and high frequencies. That is why we adopt the so called parallel computing in which more multiprocessors machines work at the same time and on the same program to both increase the amount of memory available and speed-up the results. To use parallel computing a parallel code is needed. Paper **P5** is devoted to the parallelization of the Opršal et al. (2005) code. Moreover, it is explained why we have chosen to parallelize a serial code in place of writing another one parallel in a *native form,* and are also discussed limitations that are ever present whatever will be the approach chosen for parallelizing a serial code.

In the next paragraph are shown and discussed some aspects of the parallel computing background needed for better introducing why and what should be done in dealing with the problem of parallelization, with regard of parallelization of serial codes.

4.1.1 The parallel approach

The great drawback when modeling more realistic site dynamics is the impressive computational requirements needed for numerical simulations; gigabytes of memory and gigaflop performance rates, combined with days of computational time to simulate a minute of soil shaking etc. Seismologists are being addressing these issues since nineteens (see Olsen and Archuleta (1996); Bao et al. (1996) among others), through the use of parallel computers coupled with optimization techniques such as the use of unstructured grids to reduce the number of computational nodes.

During the last 20 years a considerable amount of work has been done in numerically modeling the interaction between near-surface geological heterogeneities and seismic wave propagation (see the review of Bard (1998); Bielak et al. (1998), and references therein). The results are huge serial codes able to numerically simulate the process. It would be useful to reconvert such serial codes into parallel ones, to have more powerful simulations that realistically represent the dynamics of site effects. The paper **P5** is aimed at investigating the faster and simple way to parallelize a serial code with the ability to simulate the aforementioned interaction.

Tools to parallelize a code can be divided into high-level and low-level programming. Parallel virtual machine (PVM) and message passing interface (MPI) belong to the latter set, where the parallelization scheme is planned, designed and realized by the user. In more detail, the management of information exchanged among processors (e.g., message passing, synchronizations, etc.) is realized by the user adding code segments. Although efficient on shared and distributed memory architectures, low-level

techniques have not been considered here because too much effort (and time) must be spent to convert a serial code into an MPI (or PVM) parallel one. As it is not our aim to parallelize a serial code in such a way, we oriented our choice towards tools based on the high-level technique where all the low-level parallel machinery (creation, communications and maintenance of processes) is realized by directives to the compiler in a user-hiding mode.

The best candidates for such an approach are High Performance Fortran (HPF), OpenMP and Scalable Modelling System (SMS). It must be noticed that while OpenMP is only available on shared memory architectures, both HPF and SMS can be used in shared as well as distributed memory environments. In the present Thesis it has been preferred to adapt our code to distributed memory machines that allow to handle much larger amount of memory. We choose a high-level technique based on distributed memory architecture as it is discussed in details in paper **P5**. Because HPF is maintained by third-party and private companies (see the HPF official website http://hpff.rice.edu), the SMS tool has been chosen which is freely available (see citeGovett-et-al:2003 and the official SMS website http://wwwad.fsl.noaa.gov/ac/sms.html).

The detection of code segments that must be modified to optimize the serial code and to reduce the memory requirement is performed by the user via the application of a profiling analysis. In such a way, we can ensure a uniformly optimized serial code suitable for parallelization (see paper **P5** for details).

One of the main problems in parallel computing is the so called *load balancing,* i.e., the distribution of the computational load among processors. If it is not homogeneously distributed, there will be processors for which more time is needed for computing each time-step. As a consequence, other processors are forced to wait doing nothing, the result is a low level of performance of the parallel scheme. In such conditions it is easy that the performance of the parallel code could be even less than the serial one. A useful index for checking any gain in performance with respect to the serial code is the Speed-up, $S(n)$. It is defined as the ratio between the real time employed by one processor to run the code, $T(1)$, and the real time needed by n processors, $T(n)$:

$$S(n) = \frac{T(1)}{T(n)}$$

As an example in Fig. 4.4, the Speed-up of HPF and OpenMP-Guide are compared with ideal performance. It emerges that the Speed-up scaling is satisfactory up to 8 processors for both the approaches. Beyond this threshold the $S(n)$ tends to saturation, becoming increasingly evident for both methods, particularly with the OpenMP-Guide approach. Saturation is an important marker. To illustrate its meaning we have to consider that user-hiding message passing is a time-consuming process. Saturation starts when

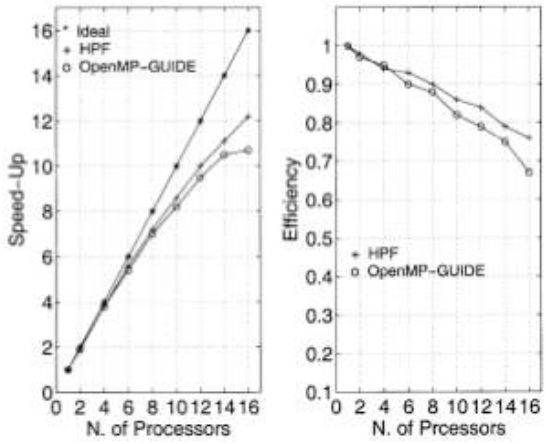

Figure 4.4: *Speed-up (left panel) and Efficiency (right panel) vs. number of processors for HPF and OpenMP compilers. Comparison shows up to 16 processors. Straight line with a asterisks represents ideal Speed-up. From Caserta et al. (2002).*

the message-passing time is comparable with the computation time needed by each processor to run its own part of the workload. The communication time increases with the number of processors while the computational time of each processor decreases. Therefore, there is no advantage in increasing the number of processors within a Speed-up saturated regime.

This is more evident from the Efficiency plot in Fig. 4.4. Efficiency, $E(n)$ is defined by the ratio between the Speed-up and the number of processors:

$$E(n) = \frac{S(n)}{n}$$

By definition, Efficiency is a measure of the relevance of user-hiding message passing for a single processor. From Fig. 4.4, it can be seen that the percentage of the total computational time spent by HPF and OpenMP-Guide in message passing is the same up to 4 processors. Beyond 4 processors, the differences increase with the number of processors.

4.2 Numerical results

We numerically simulated the soil shaking of the Valco San Paolo portion of the Tiber valley, shown in Fig. 4.2, where the 3D seismic array is located. Such a simulation has to be seen as a preliminary example of the first results of the 3D soil shaking simulations analysis. Final, detailed study will be published in a forthcoming paper.

Synthetic seismograms were extracted for the grid points corresponding to the VSC, BRH and GRB stations. In Fig. 4.5 the time histories

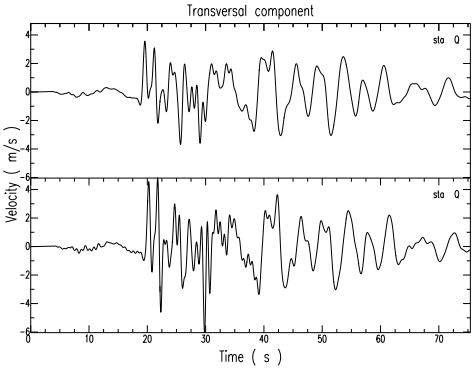

Figure 4.5: *Simulated soil shaking in GRB (top) and VSC (bottom). The component showing the best agreement with observed spectral FAS ratios has been chosen.*

of the numerically simulated ground motion for the T component of VSC and GRB stations are shown. Although the calculations were performed only for the formal time function representing an impulse response of the medium (a triangle of 0.3 seconds duration), we see that thanks to the realistic crustal model, source depth and focal mechanism the synthetics have qualitative features comparable to real data, i.e. the duration, proportion of the body- and surface-wave groups, etc. Synthetics like that cannot be however quantitatively compared with real data, but the station spectral ratios can be compared. Future calculations will be performed for a more realistic source time function, and it will be possible to study the whole time series (including their peak motion values).

In Fig. 4.6 the comparison between the smoothed FAS ratios of the recorded data and simulated synthetics are shown, together with the theoretical ratio for the 1D model of the plane-wave vertically incident excitation. The observed R component is not fitted well. We preliminarily interpret this result as a consequence of a formal limitation of the basin model in the direction along a valley (with non-reflecting boundaries). The T component is fitted better than R, mainly around the main peak at about 1.1-1.2 Hz. Nevertheless, no significant improvement in the 3D model compared the 1D one is found.

To address also the borehole, in Fig. 4.7 the observed and 3D simulated VSC/BRH spectral ratios are shown for both radial (R) and transversal (T) component. The theoretical ratio for the 1D model of the plane-wave excitation is shown as well. A good agreement at high frequencies ($> 1Hz$) between the simulated and observed ratios for the T and R component can be recognized. The agreement between 0.8 Hz and 1.0 Hz is worse, and

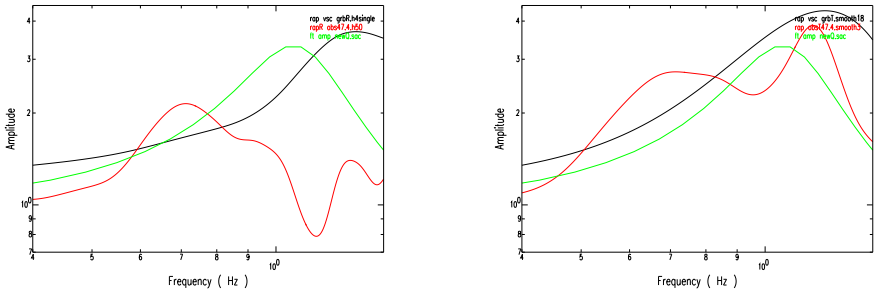

Figure 4.6: *Comparison between the FAS ratios of the radial (R) and transversal (T) component, left and right panel, respectively. They refers to observed (red curves) and simulated (black curves) of the VSC/GRB ratio of FAS. The theoretical ratio for 1D model and the plane-wave excitation is also shown (green curve).*

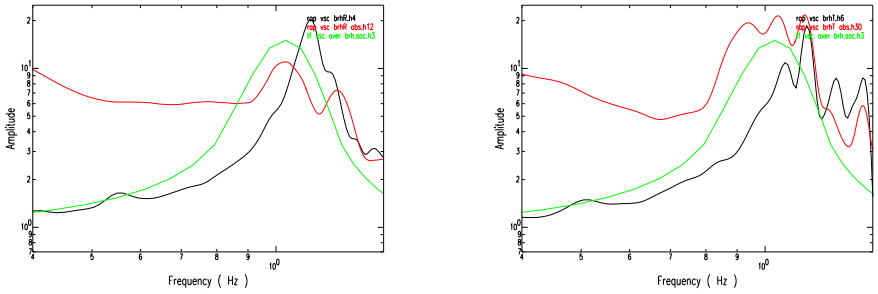

Figure 4.7: *Observed (red curves) and simulated (black curves) VSC/BRH ratios of FAS for the R component (left panel) and T component (right panel). The green curve represents the theoretical ratio for 1D model and the plane-wave excitation. The part of red curve between 0.4 and 0.7 Hz is not usable being the borehole sensor the 1Hz one.*

at frequencies f < 0.8 Hz the comparison cannot be performed because the BRH record seems not reliable due to instrumental reasons (the observed ratio does not approach value of 1 as frequency decreases). The fact that

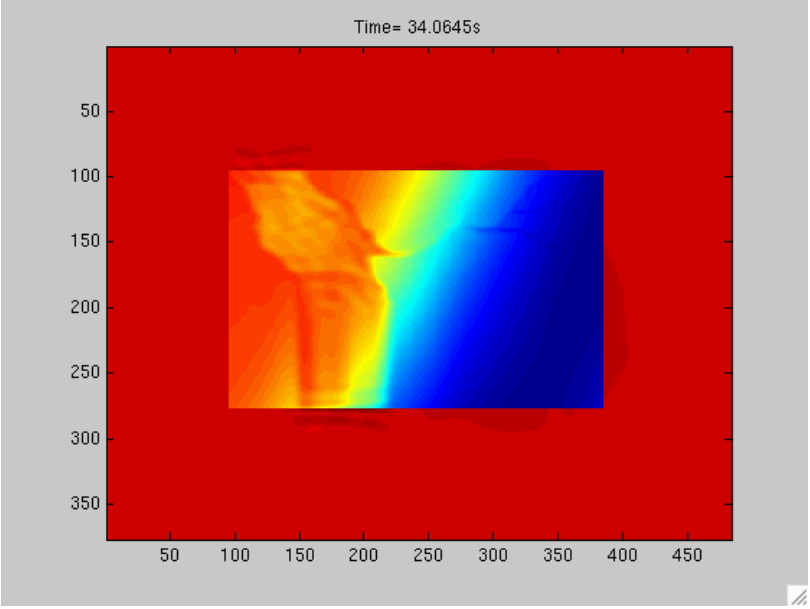

Figure 4.8: *Snapshot, from movie in the attached CD, of the soil displacement on the Tiber valley's surface. The darker is the red color and the higher is the displacement amplitude. The darker red is mainly localized at the edges of the basin. Note that the vertical axis is reversed.*

around 1 Hz the VSC/BRH ratio is fitted for both R and T, while VSC/GRB only for the T component seems to be due to the fact that the observed difference between VSC and BRH is mainly due to 1D local structure, i.e. possible 3D effects are almost the same at both the surface and the borehole station. When comparing VSC and GRB, the true 3D structure and our ability/inability to model it plays a more significant role. While the amplification around 1 Hz is mostly due to 1D structure, above 1Hz the 3D effect become probably more important, mainly at the edges of the valley.

This is better visualized by the snapshot in Fig. 4.8 where we clearly see the role played by lateral heterogeneities of the Tiber basin edges in amplifying the soil shaking. For more details see in the attached CD the full animation of the soil shaking in the Tiber valley. Calculations will be extended to 3Hz and realist time function, thus allowing a more detailed discussion.

Bibliography

Aki, K. (1957). Space and time spectra of stationary stochastic waves, with special reference to microtremors. *Bull. Earthquake Res. Inst. Tokyo Univ.*, 35:415–456.

Alessandro, C. D., Bonilla, C., Rovelli, A., and Scotti, O. (2008). Influence of site classification on computing empirical ground-motion prediction equations in Italy. In *EOS Transactio American Geophysical Unioni Fall Meeting Supplement*, volume 89.

Amato, A., Chiarabba, C., Cocco, M., Bona, M. D., and Selvaggi, G. (1994). The 1989 - 1990 seismic swarm in the Alban Hills volcanic area, Central Italy. *Journal of Volcanology and Geothermal Research*, 61:225 – 237.

Ambrosini, S., Castenetto, S., Cevolan, F., Loreto, E. D., Funiciello, R., and Liperi, L. (1986). Risposta sismica dell'area urbana di Roma in occasione del terremoto del Fucino del 13-1-1915. *Memorie della Societá Geologica Italiana*, 35:445 – 452. in Italian.

Asten, M. and Henstridge, J. (1984). Array estimators and the use of microseims for reconnaissance of sedimentary basins. *Geophysics*, 49(11):1828 – 1837.

Bao, H., Bielak, J., Ghattas, O., O'Hallorn, D., Kallivokas, L., Shewchuk, J., and Xu, J. (1996). Earthquake ground motion modeling on parallel computer. In *Supercomputing '96*, Pittsburgh, Pennsylvania, USA.

Bard, P.-Y. (1998). Microtremor measurements: a tool for site effect estimation? In *Second International Symposium on the Effects of Surface Geology on Seismic Motion*, volume 3, pages 125 – 1279, Yokohama, Japan. Irikura, Kudo, & Satani.

Basili, A., Cantore, L., Cocco, M., Frepoli, A., Margheriti, L., and Nostro, C. (1995). The June 12, 1995 microearthquake sequence in the city of Rome. *Annals of Geophysics*, 39(6):1167 – 1175.

Bettig, B., Bard, P.-Y., Scherbaum, F., Riepl, J., Cornou, C., and Hatzfeld, D. (2003). Analysis of dense array noise measurements using the modified

spatial auto-correlation method (SPAC). application to the grenoble area. *Bollettino Di Geofisica Teorica ed Applicata*, 42:281 – 304.

Bielak, J., Ghattas, O., and Bao, H. (1998). Ground motion modelling uing 3D finite element method. In *Proceedings of the 2nd International Symposium on the Effects of Surface Geology on the Seismic Motion*, pages 121 – 133, Yokohama, Japan.

Bindi, D., Luzi, L., Massa, M., and Pacor, F. (2009). Horizontal and vertical ground motion prediction equations i derived from the Italian Accelerometric Archive (ITACA). *Bulletin of Earthquake Engineering*. doi:10.1007/s10518-009-9130-9.

Bonnefoy-Claudet, S., Cornou, C., Kristek, J., Ohrnberger, M., Wathelet, M., Bard, P.-Y., Moczo, P., Fäh, D., and Cotton, F. (2004). Simulation of seismic ambient noise: I. Results of H/V and array techniques on canonical models. In *XIII World conference on Earthquake Engineering*, Vancouver, B.C., Canada.

Bonnefoy-Claudet, S., Cotton, F., and Bard, P.-Y. (2006). The nature of noise wavefield and its applications for site effects studies. A literature review. *Earth-Science Reviews*, 79:205 – 227.

Boore, D. (1983). Stochastic simulation of high-frquency ground motions based on seismological models of the radiated spectra. *Bulletin of Seismological Society of America*, 73:1865 – 1894.

Boore, D. (2005). On pads and filters: processing strong-motion data. *Bulletin of Seismological Society of America*, 95:745 – 750.

Boore, D. and Bommer, J. (2005). Processing of strong-motion accelerograms: needs, options and consequences. *Soil Dynamics and Earthquake Engineering*, 25:93 – 115.

Boschi, E., Caserta, A., Conti, C., Bona, M. D., Finiciello, R., Malagnini, L., Marra, F., Martines, G., Rovelli, A., and Salvi, S. (1995). Resonance of subsurface sediments: an unforeseen complication for designers of roman columns. *Bulletin of Seismological Society of America*, 85(1):320 – 324.

Bouchon, M. (1981). A simple method to calculate Green's functions for elastic-layered media. *Bulletin of Seismological Society of America*, 71:959 – 971.

Brocher, T. (2008). Compressional and shear-wave velocity versus depth relations for common rock types in northern California. *Bulletin of Seismological Society of America*, 98:950 – 968.

Calderoni, G., King, K., and Rovelli, A. (2009). Scaling of source spectra of the April 2009 L'Aquila, Italy earthquakes. In *EOS Transaction of American Geophysical Union*, volume 90.

Campillo, M. and Paul, A. (2003). Long range correlations in the diffuse seismic coda. *Sience*, 299:547 – 549.

Capon, J. (1969). High-resolution frequency-wavenumber spectrum analysis. In *Proceedings of the IEEE*, volume 57 (8), pages 1408 – 1418.

Caserta, A., Ruggiero, V., and Lanucara, P. (2002). Numerical modelling of dynamical interaction between seismic radiation and near-surface geological structures: a parallel approach. *Computer & Geoscience*, 28:1069 – 1077.

Caserta, A., Zahradnik, J., and Plicka, V. (1999). Ground motion modelling with a stochastically perturbed excitation. *Journal of Seismology*, 3:45 – 59.

Cauzzi, C. and Faccioli, E. (2008). Broadband (0.05 to 20 s) prediction of displacement response spectra based on worldwide digital records. *Journal of Seismology*. doi: 10.1007/s10950-008-9098-y.

Chiarabba, C., Malagnini, L., and Amato, A. (1994). Three-dimensional velocity structure and earthquake relocation in the Alban Hill volcano, Central Italy. *Bulletin of Seismological Society of America*, 84:295 – 306.

Chouet, B., Luca, G. D., Milana, G., Dawson, P., Martini, M., and Scarpa, R. (1998). Shallow velocity of Stromboli volcano, Italy, derived from small-aperture array measurements of Strombolian tremor. *Bulletin of the Seismological Society of America*, 88(3):653 – 666.

Cifelli, F., Donati, S., Funiciello, F., and Tertulliani, A. (2000). High-density macroseismic survey in urban areas. Part 2: results for the city of Rome, Italy. *Bulletin of Seismological Society of America*, 90:298 – 311.

Cornou, C., Kristek, J., Ohrnberger, M., di Giulio, G., Schissele, E., Guillier, B., Bonnefoy-Claudet, S., Wathelet, M., Fäh, D., Bard, P.-Y., and Moczo, P. (2004). Simulation of seismic ambient noise: I. Results of H/V and array techniques for real sites. In *XIII World conference on Earthquake Engineering*, Vancouver, B.C., Canada.

Fäh, D., Iodice, C., Suhaldoc, P., and Panza, G. (1993). A new method for the realistic estimation of seismic ground motion in megacities: the case of Rome. *Eartquake Spectra*, 9:643 – 667.

Florindo, F., Karner, D., Marra, F., Renne, P., Roberts, A., and Weaver, R. (2007). Radioisotopic age constraints for glacial terminations IX and

VII from aggradational sections of the Tiber River delta in Rome, Italy. *Earth Planetary Scincece Letters*, 256:61 – 80.

Frankel, A. and Vidale, J. (1992). A three-dimensional simulation of seismic waves in the Santa Clara Valley, California, from a Loma Prieta aftershock. *Bulletin of Seismological Society of America*, 82:2045 – 2074.

Gaffet, F. (1998). A dense array experiment for the observation of waveform perturbations. *Soil Dynamics and Earthquake Engineering*, 17:475 – 484.

Graves, R. (1996). Simulating seismic wave propagation in 3D media using staggered-grid finite differences. *Bulletin of Seismological Society of America*, 86:1091 – 1106.

Harjes, H. (1990). Design and siting of a new regional array in Central Europe. *Bulletin of Seismological Society of America*, 80:1801 – 1817.

Haubrich, R. (1968). Array design. *Bulletin of Seismological Society of America*, 58:997 – 991.

Hergarten, S. (2002). *Self-organized criticality in earth systems*. Springer Verlag, Berlin, Heidelberg.

Herrmann, R., Malagnini, L., and Munafó, I. (2011). Regional moment tensor of the 2009 L'Aquila earthquake sequence. *Bulletin of Seismilogical Society of America*. in press.

Horike, M. (1985). Inversion of phase velocity of long-period microtremors to the S-wave-velocity structure down to the basement in urbanized areas. *Journal of Physics of the Earth*, pages 59 – 69.

Horike, M. (1996). Geophysical exploration using microtremor measurements. In *Proceedings of the 11th World Conference on Earthquake Engineering*, Acapulco, Mexicio.

Hough, S. and Field, E. (1996). On the coherence of ground motion in the San Fernando valley. *Bulletin of Seismological Society of America*, 86:1724 – 1732.

Ishida, H., Nozawa, T., and Niwa, M. (1998). Estimation of deep surface structure based on phase velocities and spectral ratios of long period microtremors. In *Proceeding of the Second International Symposium on the Effects of Surface Geology on Seismic Motion*, pages 697 – 704, Yokoama, Japan.

Kanay, K. and Tanaka, T. (1961). On microtremors VIII. *Bulletin of the Earthquake Research Institute*, pages 97 – 114.

Karner, D. and Marra, F. (1998). Correlation of fluviodeltaic aggradational sections with glacial climate history: a revision of the classical pleistocene stratigraphy of Rome. *Geological Society of American Bulletin*, 110:748 – 758.

Karner, D., Marra, F., and Renne, P. (2001). The history of the Monti Sabatini and Alban Hills volcanoes: groundwork for assessing volcanic-tectonic hazards for rome. *Journal of Volacnology and Geothermal Reserch*, 107:185 – 219.

Kind, F. (2002). *Development of microzonation methods: application to Basle, Switzerland*. PhD thesis, Swiss Federal Institute of Technology, Zurich, Switzerland. Dissertation ETH No. 14548.

Kind, F., Fäh, D., and Giardini, D. (2005). Array measurements of S-wave velocities from ambient vibrations. *Geophysical Journal International*, 160:114 – 126.

Kvaerna, T. and Ringdahl, F. (1986). Stability of various f-k estimation techniques. In *Semmiannual technical summary*, volume 1-86/87, pages 29 – 40, Kjeller, Norway. NORSAR Scientific Report.

Lachet, C. and Bard, P.-Y. (1994). Numerical and theoretical investigations on the possibilities and limitations of Nakamura's technique. *Journal of Physics of the Earth*, 42(4):377 – 397.

Malamud, B., G.M., and Turcotte, D. (1998). Forest fires: an example of self-organized critical behavior. *Science*, 281:1840 – 1842.

Marra, F. and Rosa, C. (1995). Stratigrafia e assetto geologico dell'area romana. In *Mem. Descr. Carta Geol. Ital. La Geologia di Roma. Il Centro Storico*, pages 49 – 118. Poligrafico e Zecca dello Stato, Roma, Italy. in Italian.

Matheron, G. (1963). Principles of geostatistics. *Economic Geology*, 58:1246 – 1266.

Menke, W., Lerner-Lam, A., Dubendroff, B., and Pacheo, J. (1990). Polarization and coherence of 5 - 30 hz seismic wave fields at hard-rock site and their relevance to velocity heterogeneities in the crust. *Bulletin of Seismological Society of America*, 80:430 – 449.

Miyakoshi, K., Kagawa, T., and Kinoshita, T. (1998). Estimation of geological structures under the Kobe area using the array recordings of microtremors. In *Proceeding of the Second International Symposium on the Effects of Surface Geology on Seismic Motion*, pages 691 – 696, Yokoama, Japan.

M.N. Toksöz, Dainty, A., and Charrette, E. (1991). Coherency of ground motion at regional distances and scattering. *Physics of the Earth and Planetary Interior*, 10:53 – 77.

Moczo, P., Roveli, A., Labak, P., and Malagnini, L. (1995). Seismic response of the geological structure underlying the Roman Colosseum and a 2d resonance of a sediment valley. *Annali di Geofisica*, 38(5 - 6):939 – 956.

Molin, D. and Guidoboni, E. (1989). Effetto fonti, effetto monumenti a Roma: i terremoti dall'antichità ad oggi. In *I terremoti prima del Mille in Italia e nell'Area Mediterranea*. E. Guidoboni Editor, ING, Bologna, Italy. in Italian.

Nakamura, Y. (1989). A method for dynamic characteristics estimation of subsurface using microtremor on the ground surface. *Quarterly Report Railway Tech. Res. Inst.*, 30(1):25 – 30.

Nogoshi, M. and Igarashi, T. (1971). On the amplitude characteristics of microtremor (part 2). *Journal of Seismological Society of Japan*, pages 26 – 40.

Ohrnberger, M., Scherbaum, F., Krüger, R., Pelzing, R., and Reamer, S.-K. (2004a). How good are shear wave velocity models obtained from inversion of ambient vibrations in the lower Rhine Embayment (NW-Germany). *Bolletino di Geifisica Teorica ed Applicata*, 45(3):215 – 232.

Ohrnberger, M., Schissele, E., Cornou, C., Wathelet, M., Savvaidis, A., Scherbaum, F., Jongmans, D., and Kind, F. (2004b). Microtremor array measurements for site effect investigations: comparison of analysis methods for field data crosschecked by simulated wavefields. In *XIII World conference on Earthquake Engineering*, Vancouver, B.C., Canada.

Olsen, K. (2000). Site amplification in the Los Angeles Basin from 3D modeling of ground motion. *Bulletin of Seismological Society of America*, 90:S77 – S94.

Olsen, K., Akinci, A., Rovelli, A., Marra, F., and Malagnini, L. (2006). 3D ground-motion estimation in Rome, Italy. *Bulletin of Seismological Society of America*, 96(1):133 – 146.

Olsen, K. and Archuleta, R. (1996). Three-dimensional simulation of earthquakes on the Los Angeles Fault System. *Bulletin of Seismological Society of America*, 86:575 – 596.

Olsen, K., Day, S., and Bradley, C. (2003). Estimation of Q for long-period ($> 2s$) waves in the Los Angeles Basin. *Bulletin of Seismological Society of America*, 93:627 – 638.

Olsen, K., Pechmann, J., and Schuster, G. (1995). Simulation of 3-d elastic wave propagation in the Salt Lake Basin. *Bulletin of Geophysical Society of America*, 85:1688 – 1710.

Olsen, K. and Schuster, G. (1995). Causes of low-frequency ground motion amplification in the Salt Lake Basin: the case of the vertically-incident P wave. *Geophysicaln Journal International*, 122:1045 – 1061.

Opršal, I., Fäh, D., Mai, M., and Girdini, D. (2005). Deterministic earthquake scenario for the Basel area: simulating strong motions and site effects for Basel, Switzerland. *Journal of Geophysical Research*, 110(B4). doi:10.1029/2004JB003188.

Opršal, I., Matyska, C., and Irikura, K. (2009). The source-box wave propagation hybrid methods: general formulation and implementation. *Geophysical Journal International*, 176:555 – 564.

Opršal, I. and Zahradnìk, J. (2002). Three-dimensional finite difference method and hybrid modeling of earthquake ground motion. *ournal of Geophysical Research*, 107(B8):2161.

Opršal, I., Zahradnìk, J., Serpetsida, A., and Tselentis, G. (2004). 3d hybrid simulation of the source and site effects during the 1999 Athens earthquake. In *Proceedings of 13th World Conference on Earthquake Engineering*, Vancouver, B.C., Canada.

Pantosti, D., D'addezio, G., and Cinti, F. (1996). Paleoseismicity of the Ovindoli-Pezza fault (CentralItaly): a history including a large, previously unrecorded earthquake in Middle Ages (886 - 1300 A.D.). *Journal of Gephysical Research*, X:5937 – 5959.

Priestley, M. (1981). *Spectral analysis and time series*. Academic Press, New York, NY, USA, first edition.

Riepl, J., Oliveira, C. S., and Bard, P.-Y. (1997). Spatial coherence of seismic wave fields across an alluvial valley (weak motion). *Journal of Seismology*, pages 253 – 268.

Rovelli, A., Caserta, A., Malagnini, L., and Marra, F. (1994). Assessment of potential strong ground motions in the city of Rome. *Annali di Geofisica*, XXXVII(6):1745 – 1769.

Rovelli, A., Malagnini, L., Caserta, A., and Marra, F. (1995). Using 1-D and 2-D modelling of ground motion for seismic zonation criteria: results for the city of Rome. *Annali di Geofisica*, XXXVIII(5 - 6):591 – 605.

Rundle, J., Turcotte, D., Shcherbakov, R., W.K., and Sammis, C. (2003). Statistical physics approach to understanding the multiscale dynamics of earthquake fault systems. *Review of Geophysics*, 41(4):1019.

Salvi, S., Boschi, E., Bona, M. D., Finiciello, R., Malagnini, L., Marra, F., and Rovelli, A. (1991). Subsurface geology and variations of seismic response in the city of Rome. In EERI, editor, *Proceedings of the 4th Int. Cong. on Seismic Zonation*, volume II, Stanford, California, USA.

Satoh, T., Kawase, H., and Shin'Ichi, M. (2001). Estimation of S-wave velocity structures in and around the Sendai Basin, Japan, using arrays records of microtremors. *Bulletin of the Seismological Society of America*, 91(2):206 – 218.

Scherbaum, F. (1996). *Of poles and zeros: fundamentals of digital seismology*, volume 15. Kluwer Academic Publisher.

Schneider, J., Stepp, J., and Abrahamson, N. (1992). The spatial variation of earthquake ground motion and effects of local site conditions. In *Proceedings of the Tenth World Conference Earthquake Engineering*, pages 967 – 972, Madrid, Spain.

Scognamiglio, L., Tinti, E., Michelini, A., Dreger, D., Cirella, A., Cocco, M., Mazza, S., and Piatanesi, A. (2010). Fast determination of moment tensors and rupture history: application to the April 6th 2009, L'Aquila earthquake. *Seismological Research Letters*. submittes.

Shapiro, N. and Campillo, M. (2004). Emergence of broadband Rayleigh waves from correlations of the ambient seismic noise. *Geophysical Research Letters*, 31(7).

Sherbaum, F., Riepl, J., Bettig, B., Ohnberger, M., Cornou, C., Cotton, F., and Bard, P.-Y. (2003). Dense array measurements of ambient vibrations in the Grenoble basin to study local site effects. *EOS transaction AGU*, 80(46):F707.

Sieberg, A. (1930). Geologie der erdbeben. *Handb. Geophys.*, 84(4):550 – 555.

Singh, S., Lermo, J., Dominguez, T., Ordaz, M., Espinosa, M., Mena, E., and Quaas, R. (1988). A study of amplification of seismic waves in the Valley of Mexico with respect to the hill zone site. *Earthquake Spectra*, 4:652 – 673.

Singh, S. and Ordaz, M. (1993). On the origin of long coda observed in the lake-bed strong motions of Mexico City. *Bulletin of Seismological Society of America*, 83:1298 – 1306.

Sornette, D. (2000). *Critical phenomena in natural sciences*. Springer Verlag, Berlin, Heidelberg.

Tertulliani, A. and Riguzzi, F. (1995). Earthquakes in Rome during the past one hundred years. *Annals of Geophysics*, 38(5 - 6):581 – 590.

Tokimatsu, K. (1997). Geotechnical site characterization using surface waves. In *Proceeding of the First International Conference on Earyhquake Geotchnical Engineering*, volume 3, pages 1333 – 1368.

Valensise, G. and Pantosti, D. (2001). Database of potential sources for earthquakes larger than M 5.5 in Italy. *Annals of Geophysics*, 44. with CD-Rom.

Wald, D. and Graves, R. (1998). The seismic response of the Los Angeles Basin, California. *Bulletin of Seismological Society of America*, 88:337 – 356.

Wasten, M. and Dhu, T. (1998). Enhanced interpretation of microtremor spectral ratios using multimode Rayleigh-wave particle-motion computations. In *Proceedings of Total Risk Management in the Privatised Era*, Adelaide, Australia. Australian Earthquake Engineering Society Conference.

Wathelet, M., Jongmans, D., Ohrnberger, M., and Bonnefoy-Claudet, S. (2008). Array performances for ambient vibrations on a shallow structure and consequences over Vs inversion. *Journal of Seimology*, 12:1 – 19.

Wathelet, M., Jongmas, D., and Ohremberg, M. (2005). Direct inversion of spatial autocorrelation curves with the neighborhood algorithm. *Bulletin of the Seismological Society of America*, 95(95):1787 – 1800.

Woods, J. and Lintz, P. (1973). Plane waves at small arrays. *Geophysics*, 38:1023 – 1041.

Xia, J., Miller, R., Park, C., and Ivanov, J. (2000). Construction of 2D vertical shear-wave velocity field by the multichannels analysis of surface waves technique. In *Proceedings of the Symposium on the Application of Geophysics to Engineering and Environmental Problems*, pages 1197 – 1206, Arlington, Va., USA.

Yamamoto, H. (2000). Estimation of shallow S-wave velocity structures from phase velocities of love and Rayleigh-waves in microtremors. In *Proceedings of the 12th World Conference on Earthquake Engineering*, Auckland, New Zealand.

Yamanaka, H., Takemura, M., Hyshida, H., and Niwa, M. (1994). Characteristics of long-period microtremors and their applicability in exploration of deep sedimentary layers. *Bulletin of the Seismological Society of America*, 84(6):1831 – 1841.

Yomogida, K. and Etgen, J. (1993). 3-d wave propagation in the Los Angeles basin for the Whittier Narrows earthquake. *Bulletin of Seismological Society of America*, 83:1325 – 1344.